DISTINGUISHING CARBONATE RESERVOIR PORE FACIES WITH NUCLEAR MAGNETIC RESONANCE AS AN AID TO IDENTIFY CANDIDATES FOR ACID STIMULATION

A Thesis

by

CORALIE GENTY

Submitted to the Office of Graduate Studies of
Texas A&M University
in partial fulfillment of the requirements for the degree of

MASTER OF SCIENCE

August 2006

Major Subject: Geology

DISTINGUISHING CARBONATE RESERVOIR PORE FACIES WITH NUCLEAR MAGNETIC RESONANCE AS AN AID TO IDENTIFY CANDIDATES FOR ACID STIMULATION

A Thesis

by

CORALIE GENTY

Submitted to the Office of Graduate Studies of
Texas A&M University
in partial fulfillment of the requirements for the degree of

MASTER OF SCIENCE

Approved by:

Chair of Committee,	Wayne M. Ahr
Committee Members,	Brian J. Willis
	Jerry L. Jensen
Head of Department,	Richard L. Carlson

August 2006

Major Subject: Geology

ABSTRACT

Distinguishing Carbonate Reservoir Pore Facies with Nuclear Magnetic Resonance as an Aid to Identify Candidates for Acid Stimulation. (August 2006)

Coralie Genty, M.Eng., Ecole Nationale Supérieure de Géologie, Nancy (France)

Chair of Advisory Committee : Dr. Wayne M. Ahr

The determination of reservoir quality and its spatial distribution is a key objective in reservoir characterization. This is especially challenging for carbonates because, due to the effects of diagenesis, quality rarely follows depositional patterns. This study integrates data from thin sections and core analyses with measurements of Nuclear Magnetic Resonance (NMR) T_2 relaxation times. It exposes a novel approach to the use of NMR by applying geological and statistical analysis to define relationships between pore characteristics and the T_2 data, from which a method to identify pore origin from NMR only is developed.

One hundred and three samples taken from eleven wells located in fields of the Middle East, Alabama and Texas were used in the study. Modeling of the T_2 spectra, as the sum of three normal components, resulted in the definition of 9 parameters representing the average, the variability and the percentage of total porosity of the specific pore sizes present in the sample. Each specific pore size corresponds to one of the following genetic pore types: intergranular, matrix, dissolution-enhanced, intercrystalline, vuggy and cement-reduced. Among the 9 parameters, two variables were identified as having the highest degree of geological significance that could be used to discriminate between pore categories: μ_{max} which represents the largest average pore size of all pore types identified in the sample, and σ_{main} which represents the size variability of the most abundant pore type. Based on the joint distribution of μ_{max} and σ_{main} computed for each pore category, the probability that an unclassified sample belongs to each of the pore categories, is calculated and the sample is assigned to the category with the highest probability.

The accuracy of the method was investigated by comparing NMR predicted pore origin and genetic pore type described from thin section. A result of 89 successful predictions out of 103 samples was obtained. These promising results indicate that T_2 time can be a useful identifier of carbonate pore types. Success in this work takes us closer to identifying genetic pore types from NMR logs with minimal calibration against borehole cores and will help predict the spatial distribution of poroperm facies in complex carbonate reservoirs with much improved accuracy.

ACKNOWLEDGMENTS

First, I would like to thank my advisor, Dr. Ahr, for his constant support throughout my studies at Texas A&M, for supervising this thesis project during all its development, and for encouraging and helping me to present at the AAPG Annual Convention. I also wish to thank Dr. Jensen for his technical input on every aspect of this study, his great contribution to ensure a high quality project and his dependability whenever help was needed. This project was a very enriching experience for me. Both of you taught me a lot about how to conduct a scientific study, how to deal with a relatively new area of research and how to write and present the final results etc., always with rigor and constant desire to expose the most convincing conclusions. This allowed me the pleasure of presenting at AAPG, which was such a great opportunity and a success that I owe to both of you. I am also very grateful for the advice you gave me and the experience you shared when I had to make a decision about my future career. Finally, I wish to thank Dr. Willis for his help with checking the draft and for his very insightful comments on our work.

I am very thankful to the IFP School and the Texas A&M Petroleum Engineering Department and College of Geosciences for providing the funding for my studies here at Texas A&M. I wish to thank the International Association of Mathematical Geology for the student grant that I was awarded.

Finally, this last part of my studies was made easier thanks to the encouragement and support from my parents and my two sisters, Alice and Léonie, from the French Aggies: Nicolas, Olivier and Francois, and finally from my friends: Christina, Michele and Amber.

TABLE OF CONTENTS

Page

ABSTRACT iii
ACKNOWLEDGMENTS v
TABLE OF CONTENTS vi
LIST OF FIGURES viii
LIST OF TABLES ix
CHAPTER
I INTRODUCTION 1
Summary of the problem 1
Materials for the study 3
Objectives of the study 3
II DATA ORIGIN AND ACQUISITION 4
Geological setting of study areas 4
Permian Lower Clear Fork Formation of West Texas 5
Upper Jurassic Smackover Formation of Alabama 8
Lower Cretaceous Shuaiba Formation of the Middle East 13
Thin section data 15
Nuclear Magnetic Resonance data 15
NMR basics 15
NMR data acquisition for this study 20
III PREVIOUS WORK 22
IV METHODS OF STUDY 25
Genetic pore type classification 25
Decomposition of NMR T_2 Spectra 26
Statistical basis of the T_2 spectra decomposition 26
Equations and examples of T_2 spectra decomposition 27
Method for pore type prediction 30
V RESULTS AND INTERPRETATION 36
Rock and pore characteristics 36
Decomposition of NMR T_2 spectra 40
Pore type prediction based on probability models 41
Identification of key parameters to be used for pore type prediction 41

CHAPTER Page

Application of Bayes' theorem for predicting pore types 47
Test of the performance of the predictions 50

VI DISCUSSION 53

Thin section study limitations 53
Assumptions associated with T_2 relationship to pore-size 54
Discussion of pore type prediction method 55
Test of independence of the two key parameters μ_{max} and σ_{main} 55
Choice of 0.10 as cutoff for significant pore type component 56
Comparison of the μ_{max} and σ_{main} distributions between Adams and Shuaiba datasets 57
Interpretation of the NMR T_2 spectra decomposition 60
Applications of the pore type prediction method 62
Pore type identification from NMR measurement 62
Conditions and limitations of the pore type identification method 63
Identification of potential candidates for acid stimulation 64

VII FUTURE WORK 67

VIII CONCLUSION 69

REFERENCES CITED 71

APPENDIX A 76

APPENDIX B 79

APPENDIX C 83

APPENDIX D 88

APPENDIX E 89

APPENDIX F 94

APPENDIX G 95

VITA 97

LIST OF FIGURES

Page

Figure 1 Regional setting of the Permian Basin and location of Happy Spraberry Field..... 6

Figure 2 Stratigraphic column for the Eastern Shelf and Midland Basin during early Permian time..... 7

Figure 3 Regional setting of the southwestern part of Alabama at Upper Jurassic time, and location of Womack (1), Vocation (2) and Appleton (3) fields..... 9

Figure 4 Jurassic stratigraphy of southwestern Alabama..... 11

Figure 5 Stratigraphic column of the Lower Cretaceous of the U.A.E. region..... 14

Figure 6 Example of one NMR echo acquisition sequence, TE= inter-echo spacing..... 17

Figure 7 Example of a series of two echoes acquisition pulse sequences separated by a Tw-long re-polarization period..... 17

Figure 8 Relationship between NMR T_2 and pore size..... 19

Figure 9 Conversion of the multi-exponent decay curve into a T_2 relaxation time distribution curve..... 20

Figure 10 Conditional probability histogram for genetic pore origin..... 23

Figure 11 Genetic classification of carbonate porosity..... 25

Figure 12 Example of the decomposition of T_2 spectra for A. dissolution-enhanced, B. cemented and C. vuggy porosity..... 29

Figure 13 PDF (probability density functions) of parameter X for pore type Q_A and Q_B..... 33

Figure 14 Photographs of each of the six genetic pore types used in this study. 37

Figure 15 Univariate plots showing μ_{max} values for each pore type..... 43

Figure 16 Univariate plots showing σ_{main} values for each pore type..... 44

Figure 17 Bivariate plot of the two key parameters μ_{max} vs. σ_{main}..... 46

LIST OF TABLES

Page

Table 1 Summary of materials available for this study..... 4

Table 2 Success rates of the pore type predictions based on Bayesian probabilities..... 48

Table 3 Average Bayesian probability by which each sample was assigned to a predicted pore type..... 49

Table 4 Success rates obtained from the leave-one-out method..... 51

Table 5 Effect of varying α_{lim}= 0.10 by +/- 20% on the pore type prediction success rates..... 56

Table 6 Comparison of μ_{max} values for Adams and Shuaiba datasets..... 58

Table 7 Comparison of σ_{main} values for Adams and Shuaiba datasets..... 59

Table 8 Results from the t-test comparing σ_{main} averages between Adams and Shuaiba datasets..... 60

CHAPTER I

INTRODUCTION

SUMMARY OF THE PROBLEM

Carbonate reservoirs are more complex than clastic ones. At reservoir scale, carbonate porosity rarely follows depositional facies boundaries due to the extensive influence of diagenesis. At pore scale, carbonate reservoirs may be very heterogeneous because they have been influenced by a variety of depositional and diagenetic processes; consequently, methods other than simple recognition of depositional facies must be used to identify reservoir boundaries (Ahr et al., 2005). Moreover, reservoir characterization techniques must take into account the processes that created porosity in order to define genetic poroperm facies and rank the quality of flow units.

Interpretation of NMR measurements made on clastic reservoirs has become a successful method that is commonly used as means of overcoming the limitations of conventional wireline log interpretation methods (Henderson, 2004). From NMR logs we can, for example, determine lithology-independent porosity, estimate permeability, hydrocarbon type, and bound vs. free-fluid volumes. NMR measurements are much less commonly used to interpret carbonate reservoirs, although they have been used in some cases with a method of interpretation that was similar to applications used in the study of clastic reservoirs. The transposition of techniques used on sandstones to carbonate reservoir cases requires adapting the methods and developing specific equations, such as in Hidajat et al. (2004) where different permeability estimation methods in vuggy carbonates based on NMR response are discussed.

The existing NMR studies for carbonates reservoirs usually focus on one particular

---

This thesis follows the style and format of the American Association of Petroleum Geologists Bulletin.

field or dataset that shows a limited number of different porosity types. However it has been widely recognized that NMR curve shapes bear a relationship with pore size distribution in carbonate rocks as has already been found to be true for clastic reservoirs. Qualitative interpretation of the NMR T_2 relaxation time curves have been used to characterize the carbonate pore types and their relative abundances in samples by discriminating pore types on the basis of size (Chang et al., 1997; Ausbrooks et al., 1999; Hidajat et al., 2004).

The objective of this study is to develop a new quantitative interpretation of NMR measurements specifically for carbonate reservoirs. This study is based on the assumption that the T_2 relaxation times curve can be represented as a pore size distribution curve. Our method will enable us to identify pore types based on solely the specific NMR T_2 distribution of the rock using a genetic porosity classification. The determination of genetic pore types will be based on quantitative parameters calculated from the NMR T_2 measurements. The advantage of this method is to provide a way to identify genetic pore types from a wireline log with minimal calibration against borehole cores. This has not been possible with conventional logs that are unable to capture the small-scale heterogeneities in complex carbonate reservoirs. In contrast, the NMR response provides a potentially high enough resolution to obtain specific information about pore type and origin.

Carbonates have specific pore types and corresponding NMR responses; therefore, those correspondences should provide the chance to develop a method for interpreting pore geometry and pore origin that can be scaled-up to reservoir size. The pore types discussed in the study consist of 3 end-member carbonate genetic pore types - depositional, diagenetic and fracture, and their corresponding hybrids as defined by Ahr et al. (2005). This genetic classification allows us to take into account the origin of the porosity in our classification, so that we can later correlate in a more reliable way the specific pore categories and their attendant reservoir quality characteristics at field scale.

MATERIALS FOR THE STUDY

Forty-one borehole cores from eleven wells in four different geographic and stratigraphic locations were used in the study. All of the samples used for this study are from carbonate reservoirs. One of the fields produces from the Lower Cretaceous Shuaiba Formation of the Middle East, two fields produce from the Upper Jurassic Smackover Formation of Alabama, and one field produces from the Permian Lower Clear Fork Formation of West Texas. They were chosen because they provide a wide range of pore types that reflect differing degrees of influence by depositional and diagenetic processes. This will ensure that our method can be applied to potential future samples having about any type of porosity besides fracture porosity which was not included in the study.

OBJECTIVES OF THE STUDY

Comparison of NMR measurements with pore types and genetic categories based on data from thin sections will be examined with geostatistical methods to identify relationships between genetic pore characteristics, reservoir quality and NMR T_2 data. The resulting known genetic pore types can then be placed in a stratigraphic context to enable us to extrapolate pore categories and associated reservoir characteristics at field scale. Once the reservoir pore facies have been identified based on the interpretation of NMR, the quality of each facies can be used as a base to identify the potential candidates for acid stimulation.

CHAPTER II

DATA ORIGIN AND ACQUISITION

All of the samples used for this study are from carbonate reservoirs. This study is based on two separate datasets that come from two previous reservoir characterization studies. The first dataset is from work by Adams (2005) and represents a total of forty samples from cores taken in ten wells drilled in three different fields (Table 1). Two fields produce from the Upper Jurassic Smackover Formation of Alabama and one field produces from the Permian Lower Clear Fork Formation of West Texas. The second dataset is from work by Lodola (2004) and represents a total of sixty-three samples from one single well drilled in the Lower Cretaceous Shuaiba Formation of the Middle East (Table 1).

Table 1: Summary of materials available for this study

	Adams dataset			Shuaiba dataset
Data origin	Adams, 2005			Lodola, 2004
Field name	Happy Spraberry Field	Womack Field	Vocation/ Appleton Field	Unknown field
Geographic location	West Texas	Alabama Gulf Coast	Alabama Gulf Coast	Middle East
Formation Name	Clearfork	Smackover	Smackover	Shuaiba
Formation Age	Permian	Upper Jurassic	Upper Jurassic	Lower Cretaceous
Number of core plugs cut	6	11	23	63
Number of thin sections prepared	6	11	23	63
Number of NMR report	6	11	23	63
Number of wells represented	2	2	6	1

GEOLOGICAL SETTING OF STUDY AREAS

This chapter reviews the structural and stratigraphic setting of the three geographic and associated geological locations from which the samples were taken: Upper Jurassic

Smackover Formation of Alabama, Permian Lower Clear Fork Formation of West Texas and Lower Cretaceous Shuaiba Formation of the Middle East.

Permian Lower Clear Fork Formation of West Texas

A total of 6 samples from the Adams dataset are from the Permian Lower Clear Fork Formation of West Texas. They correspond to two wells that were drilled in the Happy Spraberry Field (Table 1).

The Permian Basin of West Texas and southern New Mexico is located in the foreland of the Marathon-Ouachita orogenic belt. This complex foreland area consists of several sub-basins that are separated by intraforeland uplifts (Figure 1). The geodynamic history of the Midland Basin started first by the deformation resulting from the Marathon orogeny that began during Mississippian time. Then the uplift of the Central Basin Platform which started in middle Pennsylvanian time added a topographic load within the orogenic foreland, causing flexure in the adjacent Midland Basin. Rapid subsidence and deformation consequently occurred in the basin until late Wolfcampian but subsidence continued until the end of the Permian. However the greatest amount of late Pennsylvanian-early Permian deposition in the Midland Basin occurs in the eastern half of the basin, opposite to the Central Basin Platform. This suggests that subsidence in the eastern Midland Basin might have been controlled mostly by shortening possibly by the Fort Chabourne fault zone located at the inflection point between shelf to basin deposits at early Permian time (Yang and Dorobek, 1995).

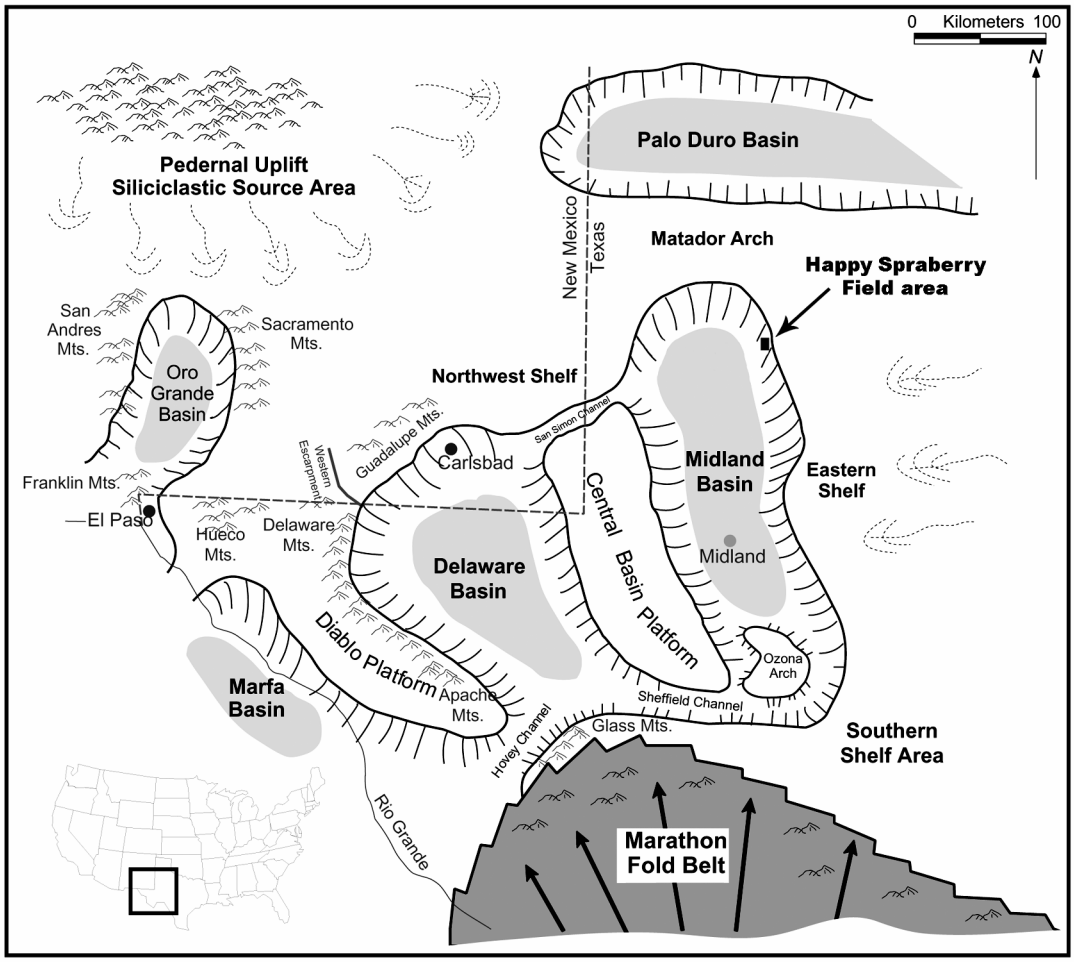

Figure 1: Regional setting of the Permian Basin and location of Happy Spraberry Field (modified after Atchley et al., 1999)

The lower Permian (Wolfcamp to Leonardian) in the northern part of the Midland Basin is divided into several formations that represent vertically stacked platform-to-basin sequences (Figure 2). Each of the formations on the shelf consists of complex facies associations of carbonates, evaporites and siliciclastics. Basin sections include interbedded shale and resedimented shelf carbonate detritus. Only the Tubb and Dean formations are dominantly sandstones and siltstones. In the Wolfcamp and lower Leonard, shelf margin and shallow-shelf patch reef facies are mainly represented by buildups and associated biograinstones. Lagoonal facies include dolomitized micrites to packstones with abundant fauna. The Wichita and Lower Clear Fork consist of stacked

to slightly offlapping rimmed-shelf deposits passing landward to shallow-shelf facies and seaward to deeper forereef slope facies. Rapidly deposited sequences of accretionary platform margin buildups developed in response to a period of increased subsidence and relative sea-level highstand. These sequences are typically composed of numerous subcycles that shoal upward to peritidal carbonate and sabkha evaporite deposits (Mazzullo and Reid, 1989).

<table>
<tr><th colspan="2"></th><th>MIDLAND BASIN</th><th>EASTERN SHELF</th></tr>
<tr><td rowspan="4">Leonardian</td><td rowspan="2">Upper Leonardian</td><td rowspan="2">Spraberry (sandstones and carbonates)</td><td>Upper Clear Fork</td></tr>
<tr><td>Middle Clear Fork</td></tr>
<tr><td rowspan="2">Lower Leonardian</td><td>Dean Sandstone</td><td>Tubb Sandstone</td></tr>
<tr><td rowspan="2">Lower Leonardian (carbonates and shales)</td><td>Lower Clear Fork</td></tr>
<tr><td>Wolf.</td><td>undivided</td><td>Wolfcamp</td><td>Wichita
Wolfcamp</td></tr>
</table>

Figure 2: Stratigraphic column for the Eastern Shelf and Midland Basin during early Permian time

Happy Spraberry Field, Garza County, Texas (location on Figure 1) was discovered in 1988 and produces oil from 15 wells. It is located on the northern part of the Eastern shelf that bounds the Midland Basin to the West. It produces from heterogeneous shallow-shelf carbonates from the Lower Clear Fork Formation of Lower Leonardian (Early Permian) age. The depositional model for the field was interpreted by Hammel (1996) and Roy (1998) and is an oolitic grainstone shoal complex associated with lithoclastics floatstones and rudstones located around patches of in situ bindstones buildups. The Happy Spraberry Field carbonates were deposited just inboard of a distally-steepened ramp. Petrophysical properties show lateral and vertical variations as a response to heterogeneities in depositional facies distribution and diagenetic overprint.

Upper Jurassic Smackover Formation of Alabama

A total of 34 samples from the Adams dataset come from the Jurassic Smackover Formation of Alabama. They are divided into 23 samples from six wells that were drilled in the Appleton and Vocation fields, and 11 samples from two wells that were drilled in the Womack field (Table 1).

Since the discovery of the Toxey Field, Choctaw County, Alabama, in 1967, Upper Jurassic Smackover carbonates have been the most productive reservoirs in Alabama (Benson et al., 1997). Jurassic sedimentation in southwestern Alabama was affected by rifted continental margin tectonics associated with the opening of the Gulf of Mexico basin in the late Triassic-Early Jurassic. Jurassic Smackover deposition in southwest Alabama has been interpreted as an ancient example of a carbonate-ramp system. It was primarily controlled by the Mississippi interior salt basin and the Manila and Conecuh embayments (Figure 3). Early salt movement as well as pre-Jurassic paleohighs such as the Wiggins uplift and Conecuh Ridge Complex caused local variations in carbonate sediment distribution (Mancini and Benson, 1980). The Louann Salt was probably responsible in forming the ramp surface.

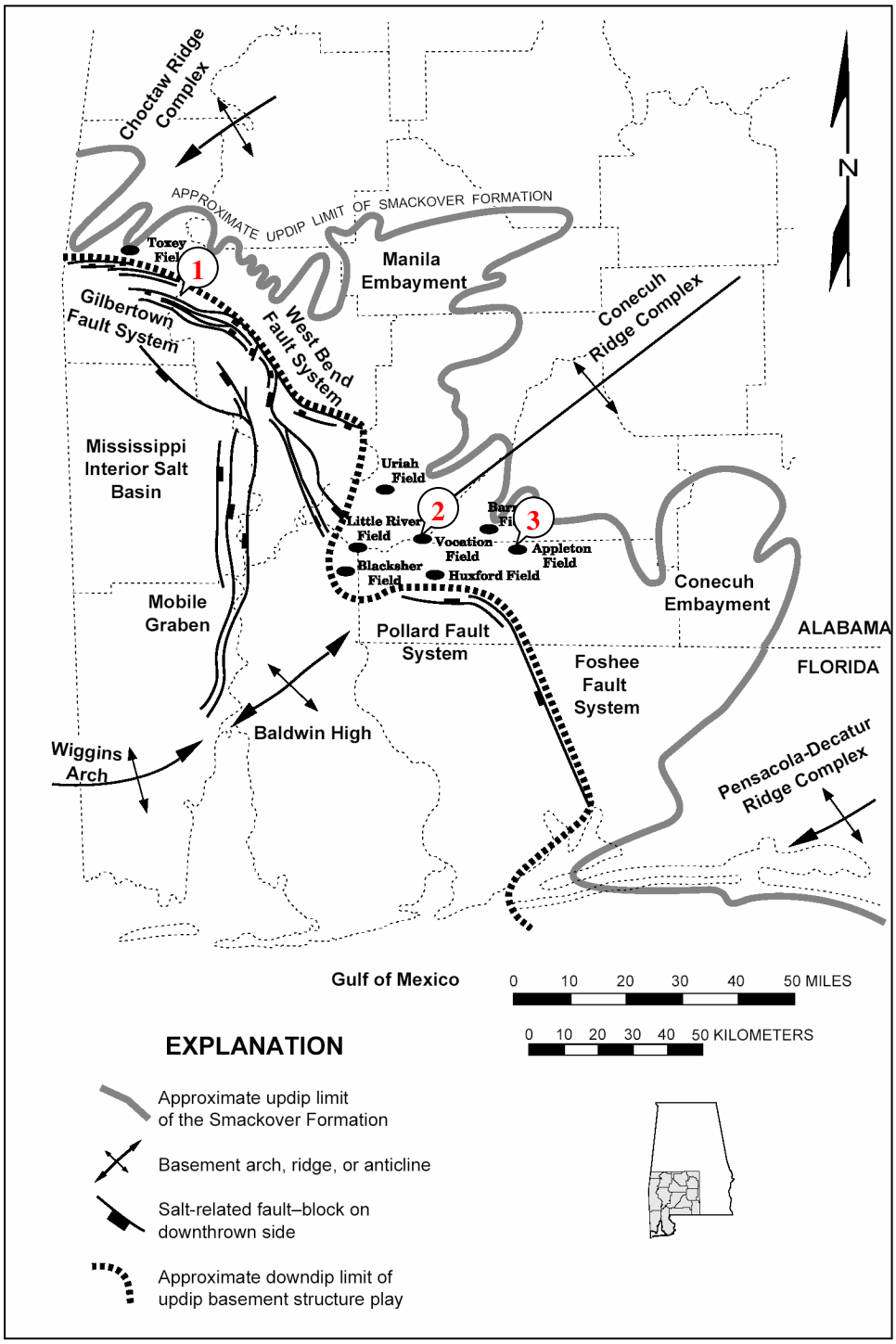

Figure 3: Regional setting of the southwestern part of Alabama at Upper Jurassic time, and location of Womack (1), Vocation (2) and Appleton (3) fields (Mancini et al., 2000)

The Smackover Formation of southwest Alabama lies between the Norphlet sandstone and the Buckner anhydrite (Figure 4). It consists of a lower transgressive unit of intertidal to subtidal predominantly mudstone lithofacies, a middle condensed unit of subtidal mudstone deposits and an upper regressive lithofacies sequence dominated by subtidal to supratidal grain-supported carbonates (Mancini et al., 1990). Petroleum traps usually combine favorable stratigraphy and structures formed by salt-related tectonic events. Grain-supported high-energy carbonates are associated with paleo-topographic highs where reservoirs are expected to be found, while low energy mudstones were deposited between these highs.

Smackover reservoirs in southwest Alabama are very heterogeneous carbonate reservoirs due to a complex history of diagenetic modification (Benson, 1985). Moreover the diagenetic sequence varies dramatically over short distances reflecting variations in paleotopography.

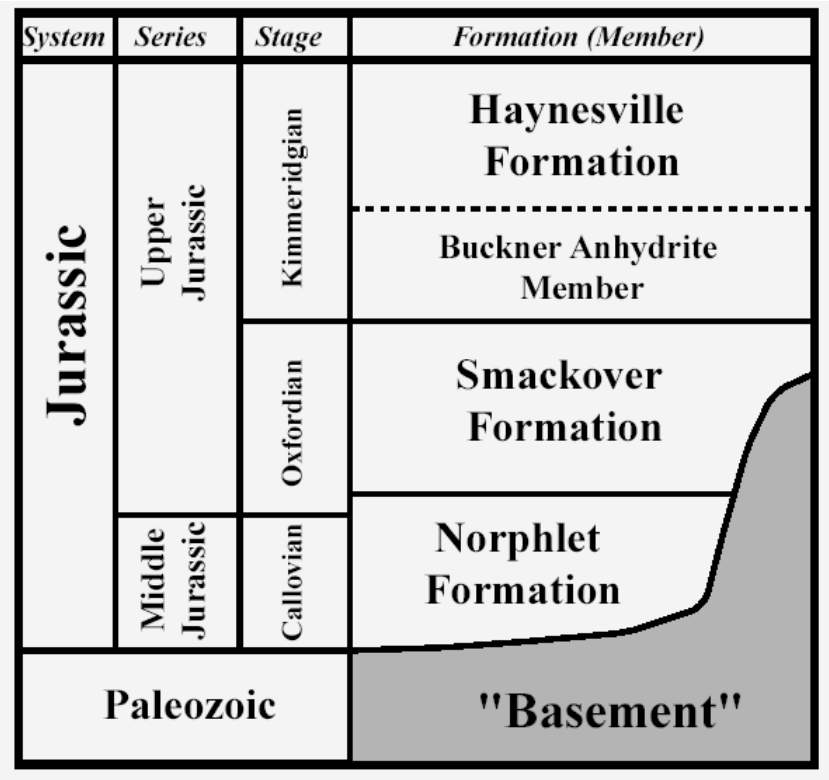

Figure 4: Jurassic stratigraphy of southwestern Alabama (Mancini et al., 2000)

Oil was discovered in the Upper Jurassic Smackover carbonate shoal complex at Womack Hill field, Choctaw and Clarke Counties, Alabama in 1970 (location on Figure 3). The Norphlet Formation overlies the Jurassic Louann Salt, which, in combination with faulting, is responsible for the petroleum trap of the field (Mancini et al., 2004). The Buckner Anhydrite Member overlies the Smackover Formation and forms the top seal in the field. All three lower, middle and upper units of the Smackover Formation described previously are present at the Womack Hill field. The reservoirs occur in vertically stacked, heterogeneous cycles that consist of lime mudstone and wackestone at the base and ooid grainstone at the top. These cycles show lateral heterogeneities in thickness, depositional texture and diagenetic fabric. Most of the production comes from the upper unit and in particular from its upper cycle which is made of lower bay and lagoonal mudstone capped by beach shoreface and shoal grainstones. Depositional fabric has the primary control on reservoir architecture but diagenesis is also a significant

factor in modifying reservoir quality. Porosity has been enhanced in particular by dissolution and dolomitization processes.

Thirty-seven wells so far have produced 31.2 MMSTB of oil which represents 36% of the original oil in place (87 MMSTB of oil) at Womack Field. A recent geological characterization and reservoir performance study enabled to define a new development strategy for the declining field in order to help sustain production (Mancini et al., 2004). It established that about 3 to 4 MMSTB of remaining oil could potentially be recovered by drilling new infill wells and perforating existing ones at strategic stratigraphic levels.

Appleton oil field located in Escambia County, Alabama, was discovered in 1983 (location on Figure 3). The field structure is a northwest-southeast-trending paleotopographic ridge composed of local low-relief paleohighs (Mancini et al., 2000). The field produces from microbial reef boundstones overlain by shoal grainstones and packstones of the Smackover Formation. Therefore, the trapping mechanism of the field is a combination of a structural component which is an anticline associated to a basement ridge, and a stratigraphic component which is the shoal and reef facies distribution. The reservoir is sealed by the Buckner anhydrites. The Smackover Formation in Appleton field principally includes the typical upper Smackover unit, composed of high-energy shoal deposits, tidal mudstones and supratidal lithologies. The middle Smackover unit consists of reef facies primarily. The traditional lower and middle Smackover units described previously are absent in this field. Although carbonate diagenesis has a significant effect on reservoir quality, carbonate depositional processes are the primary control on the geographic distribution of reef and shoal reservoirs. Hydrocarbon production has occurred mainly from the reef interval of the middle Smackover unit with contributions from the grainstones and packstones of the upper Smackover, due to higher permeability and better continuity of the reef facies.

Five wells had produced 2.7 MMSTB of oil in 2000 which represents 70% of the original oil in place (3.8 MMSTB of oil) at Appleton field. This high recovery efficiency was achieved thanks to the strong bottom-up water drive and the excellent reservoir connectivity. Since the field was approaching abandonment, a recent integrated study

helped determine a future field development strategy. It resulted in the definition of the location for a new sidetrack well in order to extend the life of the reservoir (Mancini et al., 2000).

Vocation oil field was discovered in 1971 and is part of the same play as Appleton oil field (location on Figure 3). This play regroups seven oil fields all located on paleohighs and commonly producing from Smackover carbonate reef and shoal facies. It corresponds to a Paleozoic basement high related to the Choctaw Ridge Complex of the updip basement ridge play (Figure 3). The boundaries of this play are defined by the updip limit of Smackover deposition and the regional peripheral fault trend (Mancini et al., 2000). Salt is very thin or absent in this area, therefore petroleum traps usually combine basement pre- Jurassic paleotopographic highs and favorable stratigraphy (Benson et al., 1997).

Lower Cretaceous Shuaiba Formation of the Middle East

All 40 samples from the Lodola dataset come from the Lower Cretaceous Shuaiba Formation. Data on these samples was generously provided by Schlumberger Corporation. The samples are from one well in a field in the Middle East (Table 1), but its specific geographic location is confidential.

The Shuaiba Formation forms one of the most prolific petroleum reservoirs in the Arabian Gulf. It is composed of thick, porous shelf carbonates which show considerable subsurface lateral and vertical lithofacies changes.

Alsharban et al. (2000) provide a diagenesis study of the Shuaiba Formation of the U.A.E. by using data collected from more than thirty oil and gas fields. During Cretaceous times, the central part of the U.A.E. was a wide trough oriented roughly northeast-southwest. The Shuaiba was deposited during an extensive Tethyan third-order transgression during the early to mid Aptian. The Shuaiba intrashelf basin was affected by a second-order sea-level fall in the early Aptian and was filled during the early to mid Aptian. This formation rests conformably over the carbonates of the Kharaib Formation

upper dense member and is unconformably overlain by the shale and argillaceous, silty limestone of the Albian Nahr Umr Formation (Figure 5).

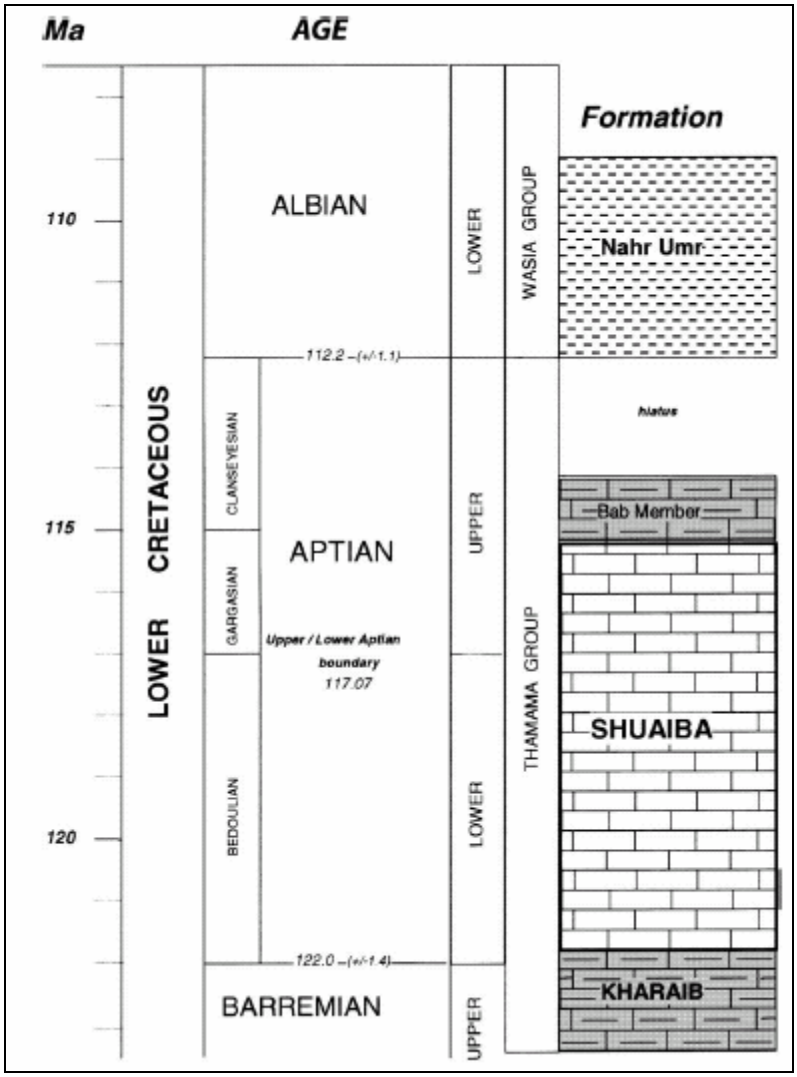

Figure 5: Stratigraphic column of the Lower Cretaceous of the U.A.E. region (Russell et al., 2002)

Alsharban et al. (2000) establish that the Shuaiba carbonates underwent various diagenetic modifications during shallow to deep burial stages. Therefore the reservoir quality of the Shuaiba Formation is highly affected by these diagenetic processes that

include stabilization of metastable carbonate phases, cementation, dolomitization and dissolution.

Russell at al. (2002) studied rock types and permeability prediction in the Bu Hasa field located in the U.A.E. and producing from the Shuaiba Formation. The Shuaiba in this field is made of shallow-water shelf carbonates and deeper water slope argillaceous limestones. This complex carbonate reservoir is characterized by geological heterogeneities related to differences in facies, texture, fauna and flora. Four different biofacies formed by rudists, corals, stomatoporoids or algae were recognized and commonly form thick and extensive biostromes. Small-scale heterogeneity causes extreme variations of petrophysical parameters, with porosities ranging from 5% to 30% and permeabilities from 0.01 mD to over 1D.

THIN SECTION DATA

The objective of this study is to compare NMR measurements with pore type and origin data from thin section analysis, in order to identify relationships between them. All 40 samples of the Adams dataset had a thin section available for petrographic study and determination of porosity type. Detailed photographs of the full thin sections were provided by Schlumberger Corporation for the 63 samples of the Shuaiba dataset, allowing us to classify genetic pore types in the same way as for the Adams dataset.

NUCLEAR MAGNETIC RESONANCE DATA

First the physical principles underlying the application of the nuclear magnetic resonance (NMR) tool will be reviewed. Then the specific conditions under which NMR data were acquired on the samples of this study will be described.

NMR basics

NMR research started in the 1940's in the area of medical sciences. The first applications of NMR in hydrocarbon reservoir studies occurred in the 1970's and measurements were conducted only in the laboratory environment. During the 1980's, a borehole NMR tool was created so that *in situ* measurements could be made.

The objective of this new tool was to provide measurements concerning the producibility of the reservoir, e.g. permeability estimation and nature of fluids, since the conventional tools do not usually provide this kind of information. As we will discuss below, the applications of NMR rely mainly on the assumption that the NMR response can be interpreted as a pore size distribution.

The NMR signal corresponds to the response of atomic nuclei to a magnetic field called $\vec{B}$. The H protons in particular act as magnets, i.e. they are originally randomly aligned in a fluid according to the local $\vec{B}$ and spin around their own axis.

The NMR tool contains a magnet that applies a strong permanent magnetic field $\vec{B}_0$. This magnetic field causes the H protons to polarize and progressively lose energy. The polarization occurs in an exponential manner, characterized by the longitudinal relaxation time constant T_1, defined as the time it takes for the fraction of polarized protons to increase from zero to 63 percent of maximum. The fraction of protons polarized at time t is equal to $1- e^{-t/T_1}$.

The NMR tool also has a receiver which can detect the signal created when the protons relax. A second magnetic field $\vec{B}_1$ is applied, which is oscillating and normal to the static magnetic field $\vec{B}_0$ (Figure 6). The H protons tip and precess about the axis of $\vec{B}_1$ and at the same frequency, called the Larmor frequency. Therefore, the aligned protons are rotated by the magnetic pulse into a plane perpendicular, or transverse, to the $\vec{B}_0$ polarization field. Free induction decay occurs when $\vec{B}_1$ is switched off i.e. the precessing H protons that were in phase, dephase rapidly and the signal at the receiver dies due to inhomogeneities in the $\vec{B}_0$ field. This decay is reversed by applying a 180° oscillating $\vec{B}$ and the protons rephase. The precession of the protons creates oscillating magnetic fields which generate a radio signal at the receiver called “echo”. This sequence of rephasing-dephasing is repeated thousands of times producing thousands of echoes acquisition sequences. However with time, the protons still lose energy and

permanently dephase, causing an exponential decrease of the echo signal. This pulse sequence is called the CMPG sequence (Carr, Purcell, Meiboom and Gill).

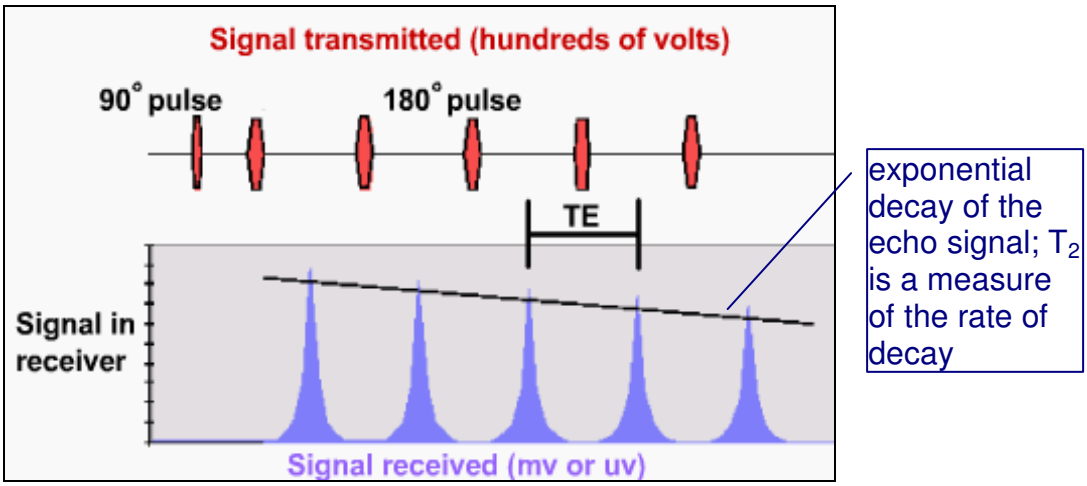

Figure 6: Example of one NMR echo acquisition sequence, TE= inter-echo spacing (Shell and Schlumberger, 1999)

Following a series of pulses, the amplitude of the signal finally becomes too small to measure and hydrogen protons must be allowed to repolarize with the permanent magnetic field (Figure 7). Pulse sequences can be customized by adapting wait time Tw, the number of pulses, and the spacing between these pulses Te.

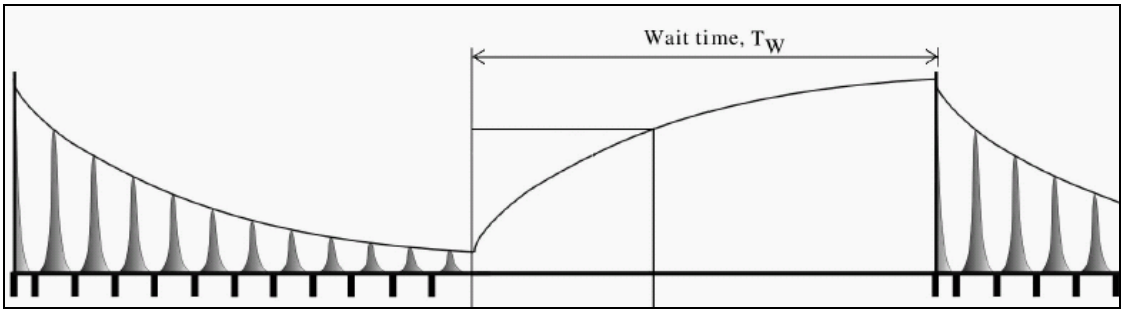

Figure 7: Example of a series of two echoes acquisition pulse sequences separated by a Tw-long re-polarization period (Henderson, 2004)

The permanent dephasing is called transverse relaxation and reflects formation properties. The exponential decrease of the echo signal is characterized by the transverse relaxation time constant T_2. T_2 is a measure of the rate at which the spinning protons loose their alignment within the transverse plane. Three relaxation mechanisms occur and affect T_2:

1. The surface relaxation corresponds to H protons colliding with the grain surface, and is a function of the pore volume and grain type.
2. The bulk fluid relaxation corresponds to H protons colliding against each other, and is a function of fluid composition and temperature.
3. The diffusion relaxation corresponds to H protons moving from one location to another that has a different $\vec{B}_0$ strength. It is caused by a non-uniform $\vec{B}_0$ and affects mainly gas.

In this study we will assume that the surface relaxation is the main cause for dephasing as all samples are fully brine-saturated (see Chapter VI for discussion), therefore the T_2 relaxation time of each fluid-filled pore can be considered to be proportional to the pore surface-to-volume ratio according to the following equation (Coates et al., 1999):

$$\frac{1}{T_2} = \rho \frac{S}{V} \quad \text{.....(1)}$$

where ρ is the ability of the surface to cause the decay of magnetization of hydrogen nuclei and is called the surface relaxivity, S is the surface area of a pore, and V is its volume. Eq. 1 assumes that surface relaxation is the dominant cause for dephasing and that the pore is small enough that self-diffusion of the liquid in the pore keeps the magnetization uniform throughout the pore as magnetization decays. This is called the fast-diffusion limit (Kenyon, 1997). These two assumptions will be discussed later in Chapter VI.

V/S has dimensions of length, therefore for pores of similar shape, *V/S* is proportional to pore size and T_2 can be considered as direct indicator of pore size (Figure 8). Fluid occupying small pores exhibits short relaxation times because of the rapid attenuation of

proton movement in close proximity to grain surfaces. In contrast, fluid in larger pores will exhibit longer relaxation times as protons are not in such close proximity to pore walls. For example, if the pores have a spherical shape of radius r, then $S/V = 3/r$ and from Eq. 1 we find that T_2 is proportional to r (Coates et al., 1999):

$$T_2 = \frac{r}{3\rho} \quad \text{.....(2)}$$

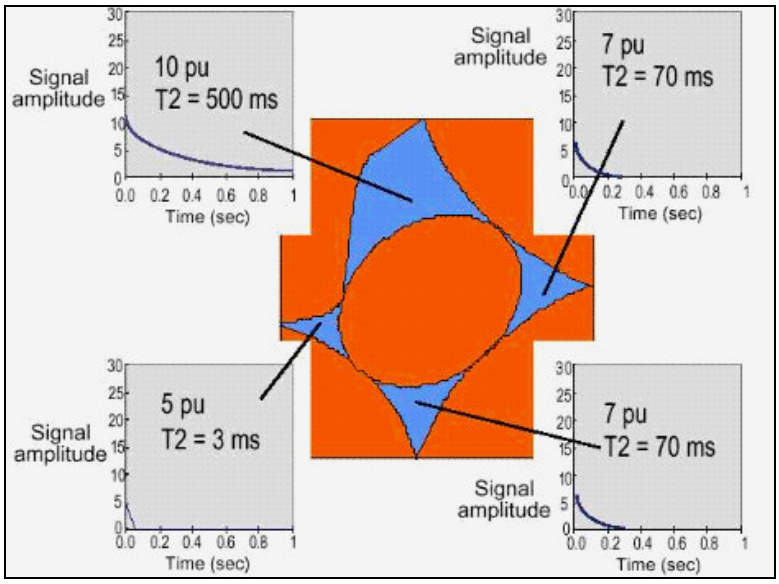

Figure 8: Relationship between NMR T_2 and pore size. The red regions are the solid and blue regions are fluid-filled voids. "pu" is porosity units, i.e. 1pu is one percent porosity (Shell and Schlumberger, 1999)

The echo signal measured by the tool is the sum of the contributions of all the pores in the volume of investigation. Typically, the formation has voids with a range of sizes, so that the echo response is a multi-exponential decay curve and is converted into a multiple decay time constant distribution curve using mathematical inversion techniques (Figure 9). This distribution curve is smoothed to obtain the T_2 distribution curve that will be interpreted as a pore-size distribution curve. Moreover, as each exponential component's amplitude is proportional to the pore volume having a particular relaxation

time, the T_2 curve amplitude is proportional to the percentage of total porosity represented by the T_2 value or pore volume.

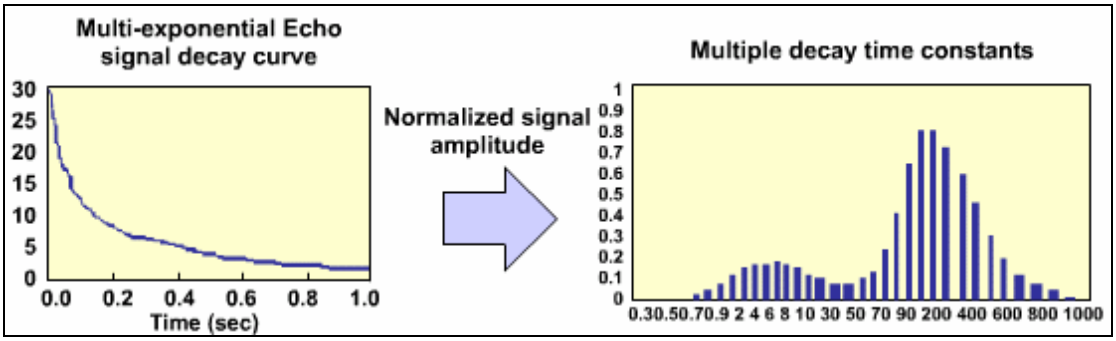

Figure 9: Conversion of the multi-exponent decay curve into a T_2 relaxation time distribution curve (Shell and Schlumberger, 1999)

The interpretation of the NMR response as a pore size distribution curve is one among many applications of NMR. Other interpretations of the T_2 distribution are mostly based on the pore-volume distribution equivalent of the T_2 curve. For example, porosity can be calculated from NMR and divided into clay-bound unmovable water, capillary-bound water, and producible free fluids. Many permeability estimation equations have also been derived based on the NMR response, both in sandstones and carbonates (Coates et al., 1997; Chang et al., 1997; Kenyon et al., 1995). Specialized pulse sequences can be used to adapt a specific application that we want to extract from the NMR signal, or to adapt a specific fluid or lithology environment in which we are acquiring NMR.

NMR data acquisition for this study

NMR T_2 relaxation time distributions were determined for the 40 samples of the Adams dataset by NUMAR Lab Services. Samples were saturated in 4% KCl brine. Each 100% brine-saturated sample was stored in an air-tight vial and measured for NMR characteristics using NUMAR's CoreSpec-1000^{TM}. The measurements were performed under a homogeneous magnetic field using 1 MHz frequency pulses at inter-echo

spacing of 0.6 and 1.2 ms (Adams, 2005). The results show that both T_2 distribution curves from the two inter-echo spacing measurements are almost identical with occasional small differences towards the lowest T_2 values. This study will use the 1.2 ms inter-echo spacing measurements.

NMR experiments were performed in Schlumberger Doll Research's NMR Laboratory for the 63 samples of the Shuaiba dataset (Lodola, 2004). The measurements were performed under a MARAN low field using 2 MHz frequency pulses at interecho spacing 0.6 ms and delay time of 10 s. The NMR measurement of the fully brine saturated samples was first; the samples were then centrifuged at two different pressures and the NMR of the partially saturated plugs was measured. However this study will use only the fully brine-saturated measurements.

CHAPTER III

PREVIOUS WORK

The idea of using NMR as an identification tool for carbonate pore types has been investigated qualitatively in some previously published studies. The T_2 distribution curve has been shown to contain information regarding pore size (expressed as fluid volume) in carbonate rocks (Kenyon et al., 1995; Chang et al., 1997; Hidajat et al., 2004). These studies typically focused on samples with a limited variety of pore types. For example, Chang et al. (1997) and Hidajat et al. (2004) interpret the shape of the T_2 curve as an indication of the relative proportions between intergranular vs. vuggy pores. However, the objective of these studies was not to use NMR to identify origin of porosity but to develop estimates of parameters such as permeability from NMR. Our study investigates the use of NMR as a method to identify the genetic categories of carbonate pores based on their size and shape characteristics.

Our study is based on Ahr's genetic classification of porosity (Ahr et al., 2005) that allows a better understanding of pore facies distribution at reservoir scale. NMR has been used previously to determine the proportion of micro-, meso- and macroporosity in sandstones (Coates et al., 1999) but never to predict origin of carbonate pore type based on T_2 distribution curve.

This study builds on the work of Lodola (2004) on the Shuaiba dataset. Our objective of relating NMR signature with pore type and origin is the same as Lodola's. However, he was using data from a single well in the Shuaiba Formation. We will extend the methods he developed and test the conclusions he made on the Adams dataset, in which there is a much greater variety of pore types. That dataset, described in Chapter II, combines samples from three different fields representing a total of ten wells (Adams, 2005).

Lodola classified his samples using three genetic pore types: depositional, facies-selective and diagenetic. He applied two different statistical approaches to attempt to relate NMR and porosity types (Lodola, 2004). Lodola's first approach used a linear combination of the T_2 distribution "descriptive statistics". He computed a variety of

statistical parameters directly from the T_2 distribution curve: variance, mean, median, mode, 90th percentile and coefficient of skewness. He determined that the mode and 90th percentile were the best two parameters for pore type discrimination, and applied Bayes' theorem to estimate the probabilities that each sample would belong to one of the three pore categories. Lodola was able to identify three critical ranges of PC1 values, PC1 being a linear combination of the mode and 90th percentile. The first range corresponds to values for which the probability for porosity to be depositional is 1 (Figure 10). The last range corresponds to values for which the probability for porosity to be diagenetic is 1. The middle range is an intermediate zone where the highest probability for porosity type is for facies-selective but the probabilities of the other two porosity types are not negligible.

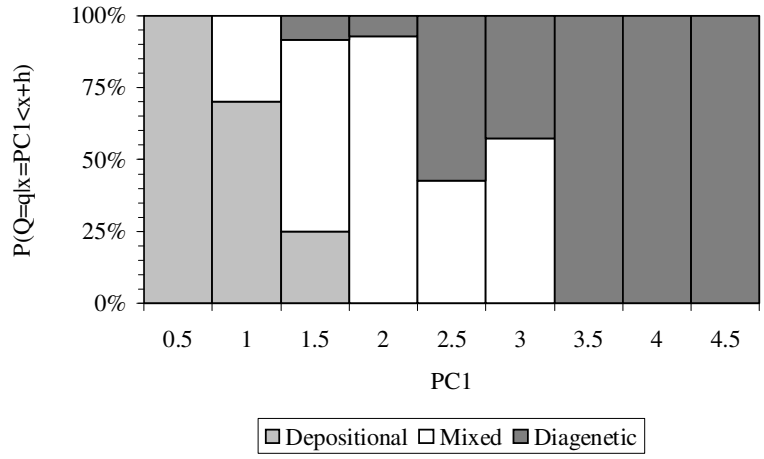

Figure 10: Conditional probability histogram for genetic pore origin. P(Q=q|x≤PC1<x+h) is the probability that pore type Q is q knowing that x≤PC1<x+h (Lodola, 2004)

The second statistical approach Lodola (2004) used was to model the log (T_2) spectrum by fitting one, two, or three normal distributions. He then assessed the improvement brought by fitting one, then two, then three normal distributions. He established that the samples with depositional pores showed almost no improvement in the fit quality, whereas using two or three distributions enabled him to reach a

significantly better fit of the NMR curve for facies selective samples, and even better for samples with diagenetic pore types. The assessment of the fit quality improvement was based on the change in coefficient of determination R^2 between model and measured T_2 curve. This result can be explained by the unimodal character of the NMR curve for depositional samples because they usually contain only one type of porosity. On the other hand, diagenetic porosity typically consists of a mix of different pore geometries resulting from the diagenetic overprint on depositional texture. Finally, using Bayes' theorem again, Lodola showed that this modeling approach also had a potential for discriminating genetic pore types by defining critical ranges on improvement of R^2 values.

Lodola investigated critical parameters calculated from the NMR curve to discriminate pore types but he did not suggest a specific method to identify the genetic pore type for an unclassified sample. He concluded that pores with different origins exhibit different T_2 characteristics; therefore, the T_2 modeling should be a reliable method to discriminate between genetic pore categories (Lodola, 2004). This study, using more data than available for Lodola's work, builds on that concept by beginning with T_2 modeling and proceeding to determine new parameters from the T_2 fitted model that can serve as more accurate pore type discriminators.

Adams studied the NMR measurements made on his dataset, however his approach was mostly qualitative. He related successfully the general shape of the T_2 curve with the genetic pore type of each sample, as well as other measurements such as pore shape from petrographic image analysis, pore throat size from mercury capillary pressure measurements, and values of petrophysical parameters measured by conventional core analysis such as porosity and permeability (Adams, 2005). He did some quantitative investigation of the NMR by matching the mode of the T_2 curve with the most abundant pore size from PIA measurements in order to interpret the NMR response in terms of pore sizes. He did not refine the use of NMR as a pore type predictor which will be the objective of this study.

CHAPTER IV

METHODS OF STUDY

GENETIC PORE TYPE CLASSIFICATION

The classification of pore types in this study was based on Ahr's genetic classification (Figure 11). First, each thin section was examined to determine which pore types were present in the sample (e.g. matrix, intergranular, vuggy, moldic etc.). Then each sample was given a unique genetic pore type. Even though different pore types might coexist in one sample, this classification by origin is restricted to the dominant process that created the porosity in that sample. As discussed previously, the strength of this genetic classification is the understanding of the origin of porosity that may help predict the spatial distribution of reservoir poroperm facies, once pore origin has been associated with reservoir quality characteristics.

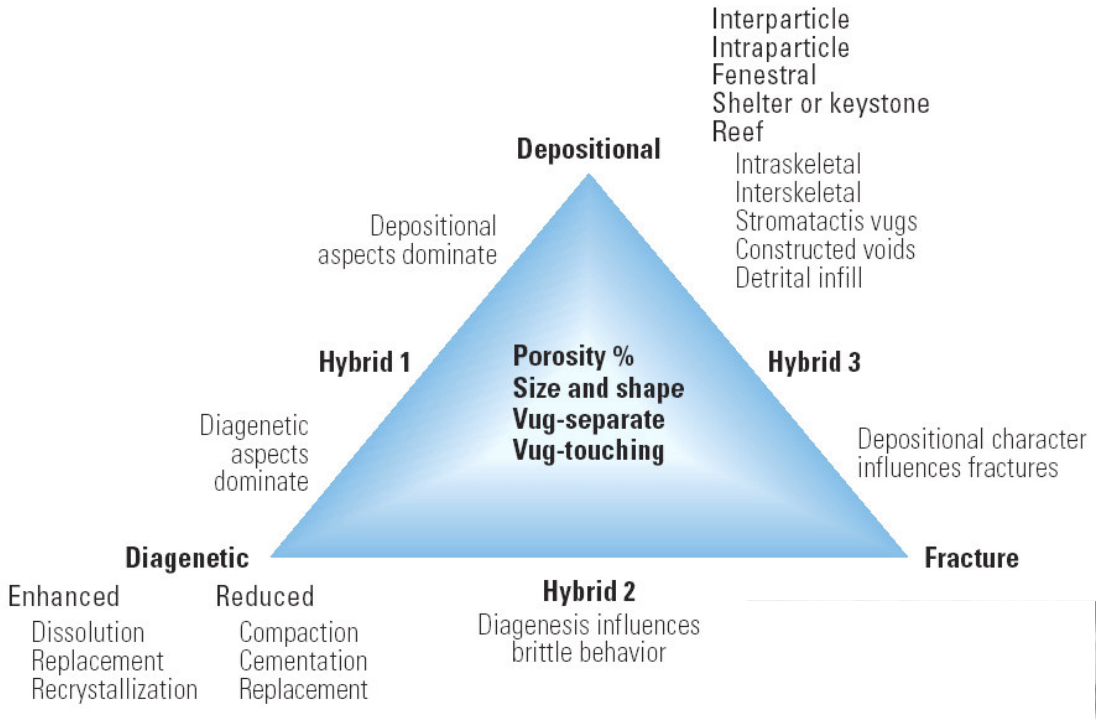

Figure 11: Genetic classification of carbonate porosity (Ahr et al., 2005)

DECOMPOSITION OF NMR T_2 SPECTRA

As described in Chapter II, the T_2 spectrum that is obtained from the NMR measurement can be interpreted as a pore-size distribution curve. Therefore, samples that contain a variety of pore types characterized by different size distributions will show a broad NMR signal, whereas samples that have only one type of pore with homogeneous pore sizes will have a narrower T_2 distribution curve. Ideally, the T_2 spectrum will show different modes corresponding to each of the main pore types present in the rock. The observed T_2 distribution will be the sum of multiple distributions, each corresponding to the size distribution of individual pore types. This suggests using a decomposition of the T_2 spectrum in order to extract the information about individual pore categories from the NMR response.

Statistical basis of the T_2 spectra decomposition

The $\log(T_2)$ spectrum of each sample f_{obs}, was approximated in this study by using the sum of three Gaussian distributions. This approach is similar to the one used by Hidajat et al. (2004). Those authors used the sum of three Weibull distributions to approximate f_{obs} and were able to relate each mode of their decomposition to one of the three pore types present in the six samples of their dataset. The choice in this study of using a sum of three Gaussian distributions to model the T_2 spectra is motivated by the following empirical and statistical considerations, based on the pore size distribution and its relationship to NMR T_2 spectra.

Several studies of carbonate porosity have shown that the log of pore size appears to be approximately normally distributed using visual inspection of the shape of the pore size distribution on a logarithmic plot (Anselmetti et al., 1998; Ausbrooks et al., 1999; Parra et al., 2002). These studies used pore size measurements made on thin sections or core photos using quantitative image analysis techniques. However, no statistical analysis was applied to test for log-normality in these examples. Results from petrographic image analysis are available for the thin sections of the Adams dataset, providing pore diameter data for all samples (Adams, 2005). Appendix A shows four

examples of log-normal probability plots to test the distribution of each pore type that was described in the Adams dataset: intergranular, dissolution-enhanced, intercrystalline and vuggy. No data are available for cemented pores since they were too small to be resolved by the optical microscope and therefore to be characterized by image analysis techniques. However, all four available plots show a nearly straight-line behavior which demonstrates that these carbonate pore sizes are log-normally distributed.

It was shown in Chapter II that T_2 relaxation time is directly proportional to pore size for pores of similar shapes, such as spherical pores (Eq. 2). This suggests that T_2 relaxation times will also exhibit the same distribution type as pore sizes, i.e. a log-normal distribution. Although carbonates typically show a great variety of pore shapes, we only need the assumption of similar shapes to hold true within one pore category since each normal component from our model will ideally characterize one pore type present in the sample. Assuming shape similarity within one specific pore category seems to be a reasonable hypothesis based, for example, on Adams study (2005), which suggests that each pore type has specific and relatively consistent shape parameters.

Therefore, based on previously published studies as well as log-normality tests of the image analysis results from Adams (2005), T_2 relaxation times for each porosity type are expected to have a log-normal distribution. Using multiple Gaussian distributions to fit the NMR T_2 curve could thus be an efficient and economical way to characterize the T_2 distribution, providing a link to the geological characteristics of the rock. If this is the case, then we would expect good to excellent fits to measured spectra and decomposition parameters which are interpretable in terms of the porosity type(s) present in each sample. This will prove to be the case, as shown later in Chapter V.

Equations and examples of T_2 spectra decomposition

The modeled T_2 spectra f_{model} is the sum of three Gaussian distributions g_i, i =1, 2, 3:

$$f_{model}(T'_2) = A\sum_{i=1}^{3} \alpha_i . g_i(\mu_i, \sigma_i^2, T'_2) \quad \text{.....(3)}$$

where f_{model} is the approximated spectrum and $T'_2 = \log(T_2)$. The values of the component relative weights α_i, means μ_i, and standard deviations σ_i, are found by minimizing the sum of squared errors calculated as follows:

$$SSE = \sum \left(f_{obs}\left(T'_{2,i}\right) - f_{model}\left(T'_{2,i}\right)\right)^2 \quad \text{.....(4)}$$

with the constraint $\Sigma\alpha_i = 1$. Thus, for each sample, f_{obs} is decomposed into three Gaussian components, each with its own weight, mean, and standard deviation. Because each mode of the T_2 decomposition ideally corresponds to a pore type in the rock, trimodal models were chosen because it is known from thin section descriptions that three genetic pore types, at most, are present in any given sample.

The objective of the decomposition is to characterize in terms of 9 or fewer parameters, the log(T_2) spectrum. Three examples of T_2 modeling for different pore types are shown in Figure 12, where the measured T_2, the modeled T_2 and the three individual normal components are shown. The parameters α_i, μ_i, and σ_i are given for each component. The decomposition reduces to two or, in some cases, a single component if the T'_2 spectrum is clearly bi- or unimodal, such as in Figure 12A and B showing respectively the T_2 decomposition for a dissolution-enhanced and cemented sample. In contrast, Figure 12C shows an example of a trimodal T'_2 spectrum which corresponds to a sample with dominant vuggy pores but also co-existing intercrystalline porosity. The fit quality is assessed by R^2.

$$R^2 = 1 - \frac{\sum \left(f_{obs}\left(T'_{2,i}\right) - f_{model}\left(T'_{2,i}\right)\right)^2}{\sum \left(f_{obs}\left(T'_{2,i}\right) - \overline{f_{obs}\left(T'_2\right)}\right)^2} \quad \text{.....(5)}$$

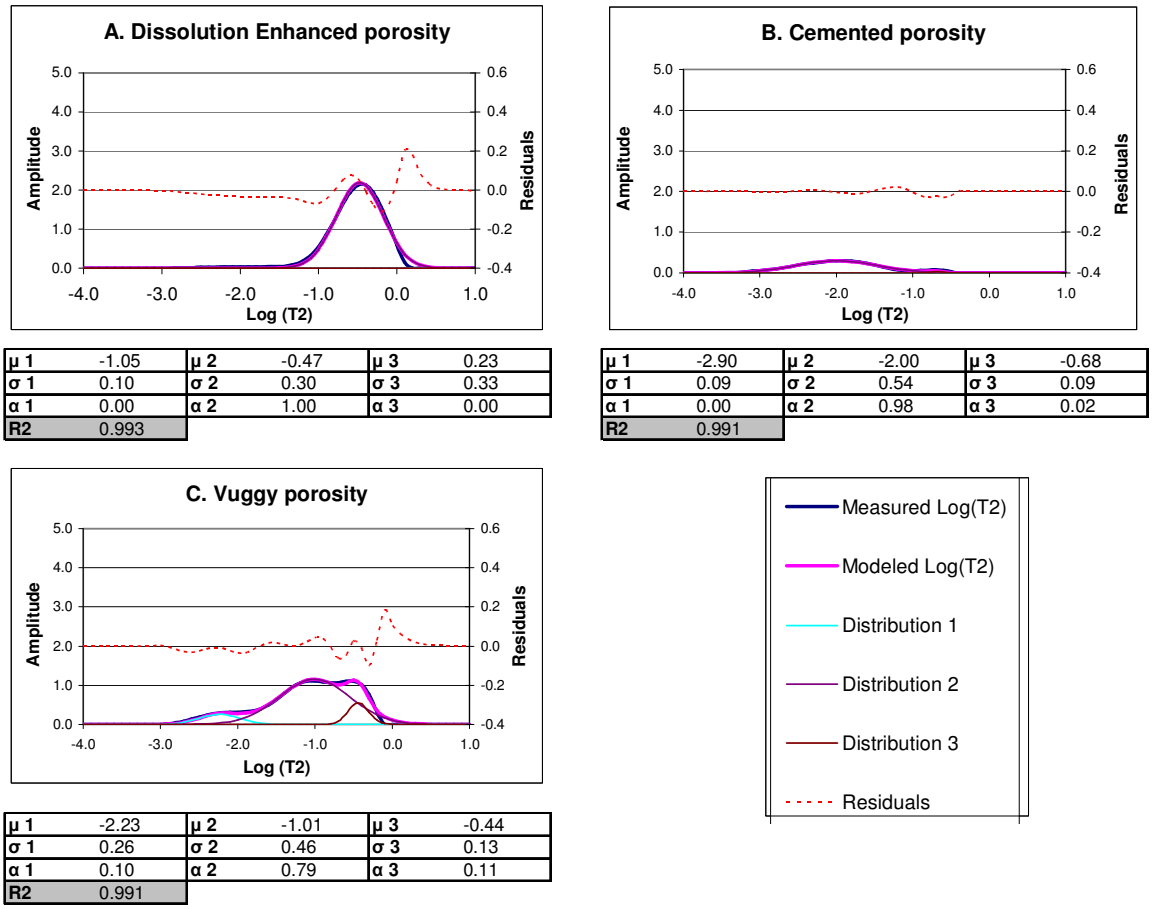

μ 1	-1.05	**μ 2**	-0.47	**μ 3**	0.23
σ 1	0.10	**σ 2**	0.30	**σ 3**	0.33
α 1	0.00	**α 2**	1.00	**α 3**	0.00
R2	0.993				

μ 1	-2.90	**μ 2**	-2.00	**μ 3**	-0.68
σ 1	0.09	**σ 2**	0.54	**σ 3**	0.09
α 1	0.00	**α 2**	0.98	**α 3**	0.02
R2	0.991				

μ 1	-2.23	**μ 2**	-1.01	**μ 3**	-0.44
σ 1	0.26	**σ 2**	0.46	**σ 3**	0.13
α 1	0.10	**α 2**	0.79	**α 3**	0.11
R2	0.991				

Figure 12: Example of the decomposition of T_2 spectra for A. dissolution-enhanced, B. cemented and C. vuggy porosity. The purple curve corresponds to f_{model}, and the dark blue curve to f_{obs}. The R^2 values close to 1 show that f_{obs} is closely matched by f_{model}

The minimization of SSE (Eq. 4) to obtain weights α_i, means μ_i, and standard deviations σ_i, includes a "penalty term". This penalty term is a coefficient that is proportional to the weights α_i of the components. Its effect is to increase SSE when the total number of components from the decomposition, which is between 1 and 3, increases. The purpose of the penalty function is to minimize the number of final components as long as the degree of fit between modeled and measured T_2 spectra has an R^2 value greater than 0.99. Therefore, the T_2 model with fewest components is "privileged", which helps extract the portions of the spectra that represent pore types that contribute most to the reservoir quality. This "simplification" is necessary in order to assign only one genetic pore type to each sample based on the NMR response that is

compared with the genetic pore type determined from the thin section description. This synthetic approach will be supported by the results presented in Chapter V and will be discussed in Chapter VI.

METHOD FOR PORE TYPE PREDICTION

The decomposition of the $\log(T_2)$ spectrum enables one to extract components that might be interpreted as different individual pore categories coexisting in one sample. Based on the parameters that result from the decomposition, namely the component relative weights α_i, the means μ_i, and the standard deviations σ_i (Eq. 3), a quantitative method can be developed which assigns a genetic pore type to an unclassified sample.

The first step in developing this method or pore type prediction is to identify the key parameters among the α_i, μ_i, and σ_i available that serve as best discriminators for pore types. The geological significance of these values is interpreted as follows. For each pore type present in the rock, represented by the i^{th} component, i = 1, 2, 3, the weight α_i represents the percentage of total porosity contributed by this pore type, the average μ_i is proportional to the size of this pore type, and the standard deviation σ_i is the variability of this pore size. The parameters most likely to reflect the specificities of the T_2 spectra related to the pore type characteristics are then tested. Univariate and bivariate plots are used in this study to visualize the discriminatory power of the parameters α_i, μ_i, and σ_i among pore categories. A discrimination routine from the module STEPDISC of the statistics software SAS provides an independent, statistical method, of identifying which linear combination of the 9 parameters provides the best discriminator. This routine identifies the parameters with the best discriminatory power based on a statistical F-test. The value of the geologically-based method is that it uses geological arguments to identify which of the 9 parameters are important for pore type rather than leaving the choice to satisfy a statistical criterion. Invoking geological-based choices makes for a method which is much more likely to be successful in evaluating samples which are not in the current datasets.

Once the key parameters have been identified, a prediction method based on Bayes' theorem can be employed. This theorem allows one to calculate the probability that a particular sample belongs to a given pore category, knowing the values of the identified key parameters. This powerful method is very common for decision-based procedures (Krzanowski, 2000) and requires the use of conditional probabilities.

Conditional probabilities are a simple extension of the familiar concept of probability. The conditional probability, P(A|B) and read as "the probability that A occurs given that B has occurred", captures the fact that information can change one's perception about the likelihood of something occurring. For example, suppose that A = the porosity is 18%. The likelihood of the formation having an 18% porosity, P(A), could change if something was known about the bulk density measurement (event B) at that location. If B = 2.40 g/cc, the 18% porosity is very likely, if B = 2.70 g/cc, the 18% is less likely. P(A|B) provides a way of recognizing that link between events A and B.

As it happens, P(A|B) and P(B|A) are related and Bayes' theorem gives the relationship: $P(A|B) = P(B|A) \times [P(A)/P(B)]$. So, continuing with the same example, Bayes theorem can be used to give the probability of 18% porosity, given a measured bulk density of 2.40 g/cc, in terms of the probability of measuring 2.40 g/cc when the formation has 18% porosity. One could use a number of 18% porosity samples and measure their densities to obtain P(B|A). Then, when the density of a new sample is measured to be 2.40 g/cc, the likelihood that the sample has 18% porosity can be calculated. Using probabilities, there is no need for an exact, mathematical relationship between density and porosity. The price paid for avoiding the mathematical relationship is that density and porosity have to be measured on a number of samples and wrong probabilities might be obtained because too few samples have been measured.

The NMR—pore type problem of this study boils down to exactly this approach because there is no deterministic relationship between pore type and NMR response. Each pore type is described from thin section and the NMR response – of the rock plug from which the thin section was cut - is measured (now A is the pore type of the sample and B is one or more characteristics of the T_2 distribution measured from that sample),

giving the probability P(B|A). Then Bayes' theorem is applied to compute P(A|B). Finally, with a new specimen, the NMR response, B, is measured to estimate the probability of that sample of having a particular pore type, A. Of course, several possible pore types and several characteristics of the NMR measurement need to be taken into account in this study; therefore the math gets more complicated.

Bayes' theorem applied to probability calculation for pore type Q_A is:

$$P(S_{\boldsymbol{i}} \in Q_A \,|\, par. = R) = \frac{P(par. = R \,|\, S_{\boldsymbol{i}} \in Q_A) \times P(S_{\boldsymbol{i}} \in Q_A)}{\sum_S P(par. = R \,|\, S_{\boldsymbol{i}} \in Q_S) \times P(S_{\boldsymbol{i}} \in Q_S)} \quad \text{.....(6)}$$

with:

$P(S_{\boldsymbol{i}} \in Q_A \,|\, par. = R)$ is the probability that sample $\boldsymbol{i}$ belongs to pore category Q_A knowing that the key parameters ("*par.*") are equal to *R*. $P(S_{\boldsymbol{i}} \in Q_A \,|\, par. = R)$ is estimated based on the following probabilities. First $P(S_{\boldsymbol{i}} \in Q_A)$ is the probability that sample $\boldsymbol{i}$ belongs to pore category Q_A. It is also called a-priori probability, as it corresponds to the probability of a sample picked randomly to belong to one pore category not using yet the value of any specific measurement made on the rock. Then $P(par. = R \,|\, S_{\boldsymbol{i}} \in Q_A)$ is the probability that the key parameters are equal to *R* knowing that sample $\boldsymbol{i}$ belongs to pore category Q_A. This probability will be estimated by assuming that the key parameters have a joint-normal distribution.

In the case where it is assumed that a single key parameter X exists from which one can discriminate pore categories (Figure 13), the normal probability density function $f_{QS}(x)$ of each pore category Q_S for the variable X is estimated based on sample mean and variance computed from the data available for each pore type. $P(par. = R \,|\, S_{\boldsymbol{i}} \in Q_S)$ becomes $P(X = x_i \,|\, S_{\boldsymbol{i}} \in Q_S)$ that can be estimated as follows:

$$P(X = x_i \,|\, S_{\boldsymbol{i}} \in Q_S) = \int_{dx} f_{Q_S}(x).dx \approx f_{Q_S}(x).dx \quad \text{.....(7)}$$

with *dx* being a small interval of variation of X.

For example, consider the situation where there are only two pore types Q_A and Q_B and one key parameter X (Figure 13). $f_{QA}(x)$ and $f_{QB}(x)$ are respectively the normal probability density functions of X for pore type A and pore type B samples. x_1 is the value of X measured on sample 1.

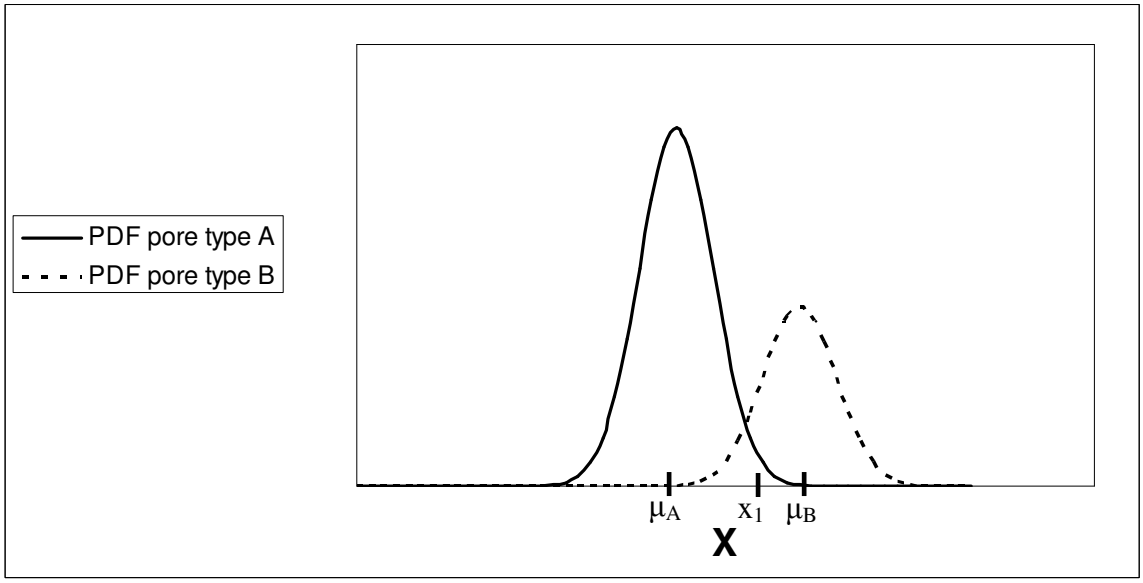

Figure 13: PDF (probability density functions) of parameter X for pore type Q_A and Q_B. These PDFs are used to estimate probability that sample 1, for which $X=x_1$, belongs to Q_A or Q_B

Therefore, the probability that sample 1 belongs to pore category Q_A is estimated based on Eq. 6:

$$P(S1\in Q_A \,|\, X=x_1)=\frac{P(X=x_1 \,|\, S1\in Q_A)\times P(S1\in Q_A)}{P(X=x_1 \,|\, S1\in Q_A)\times P(S1\in Q_A)+P(X=x_1 \,|\, S1\in Q_B)\times P(S1\in Q_B)}$$

with $P(X=x_1 \,|\, S1\in Q_A)=\int_{dx} f_{Q_A}(x).dx \approx f_{Q_A}(x).dx$

and $P(X=x_1 \,|\, S1\in Q_B)=\int_{dx} f_{Q_B}(x).dx \approx f_{Q_B}(x).dx$

that are calculated assuming normal probability density functions $f_{QA}(x)$ and $f_{QB}(x)$.

In the 2D-case, it is assumed that two key parameters X and Y can be identified and on which the pore type discrimination will be based. Therefore calculations can be made of the joint normal probability density function $f_{QS}(x,y)$ of each pore category Q_S for the two variables X and Y. This will enable the calculation of $P(par. = R \mid S\,\mathbf{i} \in Q_S)$ that is now $P(X = x_i, Y = y_i \mid S\,\mathbf{i} \in Q_S)$ as follows:

$$P(X = x_i, Y = y_i \mid S\,\mathbf{i} \in Q_S) = \iint_{dx,dy} f_{QS}(x, y).dx.dy \approx f_{QS}(x, y).dx.dy \quad \text{.....(8)}$$

with *dx* and *dy* being small intervals of variations of X and Y. The joint normal probability density function of two normally distributed parameters X and Y is calculated as follows:

$$f(x, y) = \frac{1}{2\pi\sigma_X \sigma_Y \sqrt{1-\rho^2}} \exp\left[-\frac{x^{*2} - 2\rho x^* y^* + y^{*2}}{2(1-\rho^2)} \right] \quad \text{.....(9)}$$

where $x^* = \frac{x - \mu_X}{\sigma_X}$, $y^* = \frac{y - \mu_Y}{\sigma_Y}$ and $\rho = \frac{Cov(X,Y)}{\sigma_X \sigma_Y}$ (correlation coefficient between X and Y)

Once the probability density functions are computed for each pore category, the probability of an unclassified sample belonging to a given pore category is estimated based on Eq. 6. Finally, the unclassified sample is assigned to the pore category associated with the highest probability.

Some alternatives to this method of pore type prediction could be considered. For example, the distance of each sample to the mean of each pore category could be calculated as a way to predict pore type, by assigning an unclassified sample to the pore category that has the closest mean value to the sample value. It would still be possible to incorporate several key parameters by calculating a multivariate mean. However the computation of simple Euclidian distance would not take into account the standard deviation of the key parameters for each pore category like the Bayesian approach allows (see σ_X and σ_Y in Eq. 9). Another method that permits the incorporation of as many parameters as one might wish is the method of neural networks. Neural networks

have the flexibility to combine the T_2 parameters in non-linear fashions to provide for better prediction. However, such networks usually require large datasets and, thus, may not be suitable for this study because the Adams dataset contains too few samples for some of the pore categories (see Chapter V). Furthermore, the applicability and robustness of neural networks outside of the dataset for which they are developed is often limited (e.g., Bui et al., 2006).

CHAPTER V

RESULTS AND INTERPRETATION

ROCK AND PORE CHARACTERISTICS

The classification of pore types based on thin section study was established in the two previous studies from which our two datasets derive (Lodola, 2004; Adams, 2005).

Six genetic pore types were observed in the samples:

- **Matrix**: microporosity contained in the matrix and formed at the time of deposition
- **Cemented**: porosity that has been reduced by cementation
- **Intergranular**: porosity in between the grains, formed at time of deposition
- **Dissolution-enhanced**: porosity that has been created by dissolution, comprising moldic pores (preferential dissolution of skeletal grains or ooids) and intercrystalline pores that were slightly enlarged by dissolution
- **Intercrystalline**: porosity in between the dolomite crystals after complete replacement by dolomite
- **Vuggy**: porosity that has been enlarged by dissolution to the extent that vugs are larger than surrounding constituent particles.

Figure 14 shows an example of each genetic pore type from any of the four geographical locations where our samples come from.

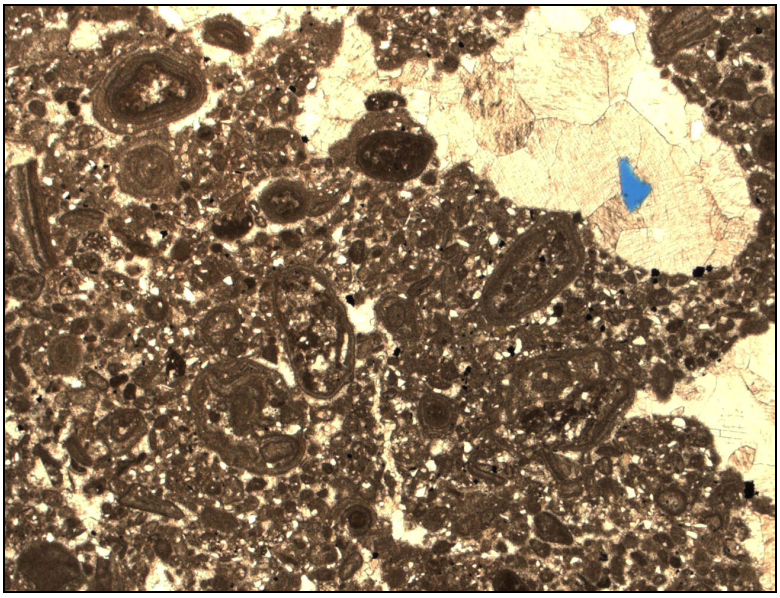

A. Appleton Field, Sample 12,868

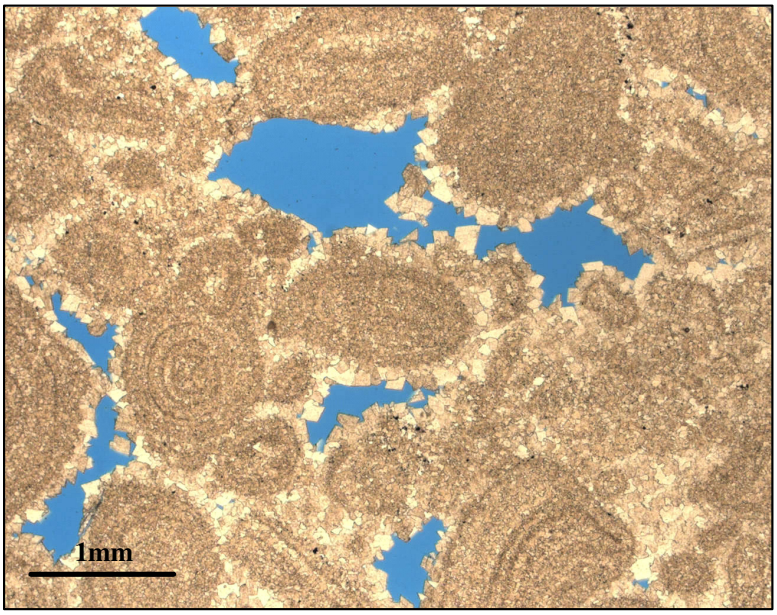

B. Vocation Field, Sample 14,017

Figure 14: Photographs of each of the six genetic pore types used in this study. A: Cemented, B: Intergranular, C: Dissolution Enhanced, D: Intercrystalline, E: Vuggy, F: Matrix (Lodola, 2004; Adams, 2005)

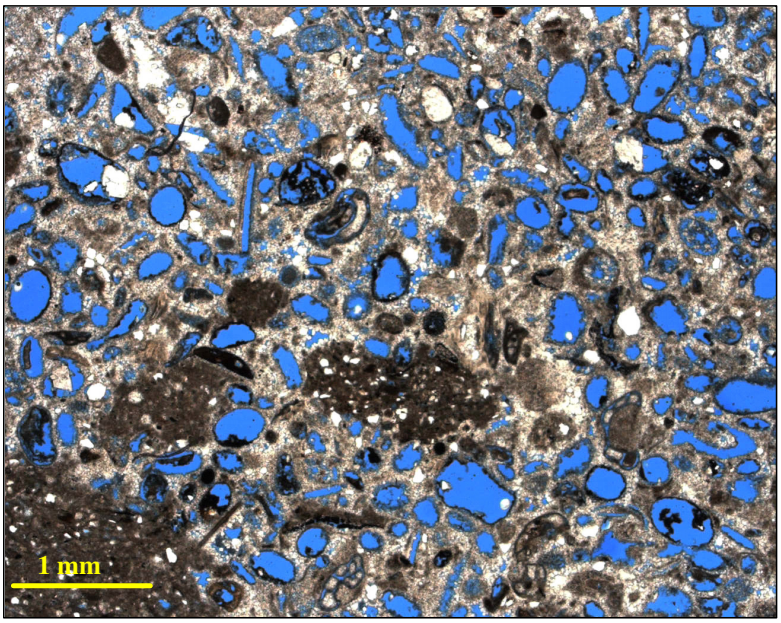

C. Happy Spraberry Field, Sample 4925

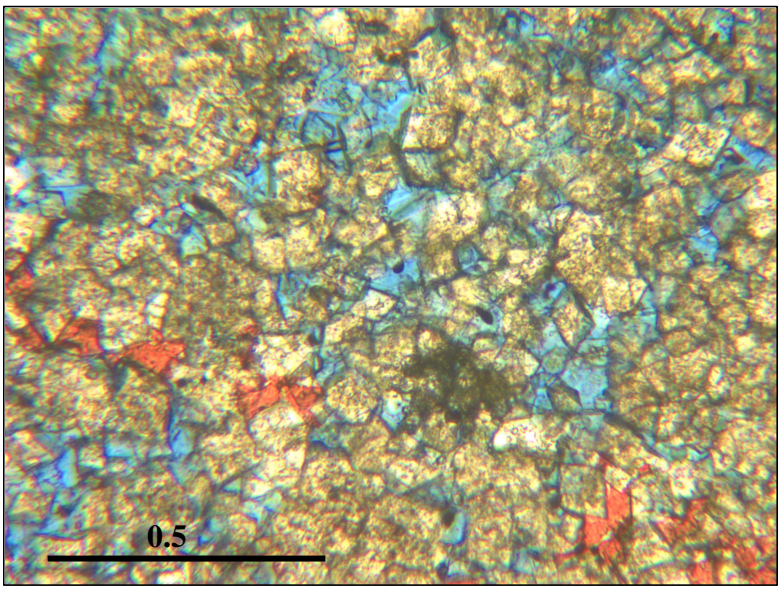

D. Womack Hill Field, Sample 11,192

Figure 14: (Continued)

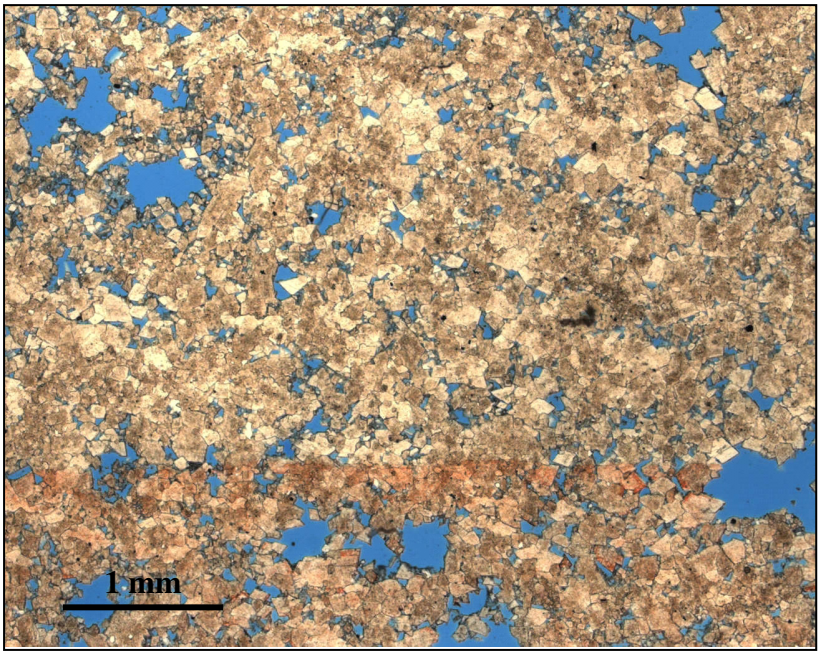

E. Appleton Field, Sample 12,964

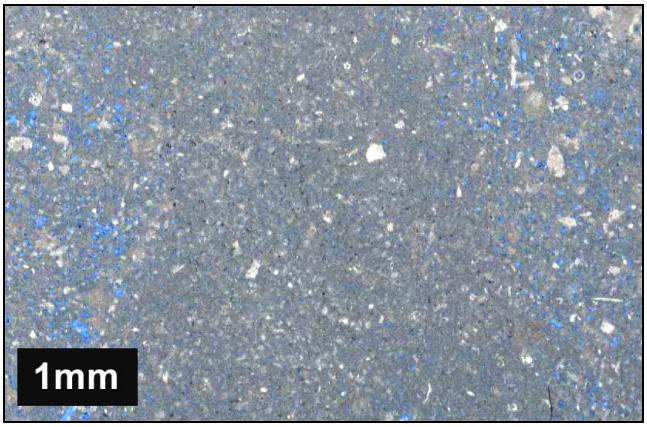

F. Shuaiba well, Sample 8396.50

Figure 14: (Continued)

As described in Chapter II, the Happy Field reservoirs consist of shallow-shelf carbonates from the Permian-aged, Lower Clearfork Formation. The reservoir facies consist of an oolitic grainstone and skeletal packstone accumulation that is laterally equivalent to scattered, *in situ* bindstones buildups. The six samples from Happy Field exhibited cemented and dissolution-enhanced pore types. The classification of these six samples together with well name and sample depths are listed in Appendix B.

Womack Hill Field, Alabama, produces mainly from lagoonal mudstones capped by strandplain shoreface grainstones of the Upper Jurassic Smackover Formation. The reservoir occurs in vertically stacked heterogeneous parasequences that consist of muddy facies at the base and ooid grainstones at the top. The eleven samples from Womack Hill Field exhibited dissolution-enhanced, intercrystalline and vuggy pore types (Appendix B).

Appleton and Vocation fields produce from microbialite bindstones of the middle Smackover unit along with overlying shoal grainstones and packstones of the upper Smackover unit. The twenty-three samples from the Appleton and Vocations fields showed cemented, intergranular, dissolution-enhanced, intercrystalline and vuggy pore types (Appendix B).

Textures present in the Shuaiba samples consist of coarse-grained carbonates in the upper half (dominantly packstones and grainstones), with mudstones and wackestones dominant towards the bottom of the section. Matrix microporosity and skelmoldic porosity from dissolution of rudist fragments are present in almost all of the samples, whether they are the dominant contributor to total porosity or not. The sixty-three samples from the Shuaiba dataset exhibited matrix, dissolution-enhanced and vuggy pore types (Appendix B).

DECOMPOSITION OF NMR T_2 SPECTRA

Results of the NMR T_2 spectra decomposition of both Adams and Shuaiba datasets are listed in Appendix C. For all T_2 spectral decompositions, the modeled T_2 were found to closely correspond with measured T_2 values. Calculated values for R^2 (Eq. 5), range

from 0.95 to 1.0 (Appendix C and Figure 12), showing that Gaussian distributions provide a good to excellent fit to measured T_2 spectra.

PORE TYPE PREDICTION BASED ON PROBABILITY MODELS

Identification of key parameters to be used for pore type prediction

The initial T_2 spectral decomposition produced relative weights α_i, means μ_i, and standard deviations σ_i for each sample (Chapter IV: Eq. 3). As discussed previously, geological interpretations of the significance of these values are as follows. For each pore type represented by a single normal component i, the weight α_i represents the percentage of total porosity contributed by that pore type; the average μ_i is proportional to the specific volume of that pore type, and the standard deviation σ_i represents the variability of that pore volume.

In addition to these nine values characterizing the T_2 spectrum, two further values of geological significance were produced from the existing nine values. The two variables μ_{max} and σ_{main} obtained from the T_2 decomposition were added to the calculations because they were found to correspond closely with two genetic characteristics of pores.

The first parameter, μ_{max}, corresponds to the maximum mean μ_i that has a significant weight; that is, a weight with a value $\alpha_i > 0.10$. The choice of this "cutoff value" $\alpha_{lim} = 0.10$ will be discussed in Chapter VI. μ_{max} corresponds to the largest average pore size of all genetic pore categories identified by the T_2 spectra decomposition. Cemented pores are characterized by their low μ_{max}; the low value indicates that the pore volume has been reduced by cementation (Figure15A). Vuggy pores are identified by their high $\mu_{max,}$ which indicates that they have been enlarged by dissolution that was not limited by mineral or particle size (Figure15A and B). Note that μ_{max} does not necessarily correspond to the average size of the pore type that has the greatest abundance (largest α) in the sample, but to the pore type that has the largest average size. The component with the largest α is called the *main component* and corresponds to the most abundant genetic pore type in the sample. For example, samples with vuggy pores typically show decompositions with both a main component and a secondary component approaching

the maximum T_2 values for the sample (Figure 12C). The presence of high values for main and secondary components is due to the fact that vugs are not the dominant pore type in these particular rocks; a significant part of the signal is related to a second pore type. All the vuggy pores in this sample collection are from extensively dolomitized rocks that also exhibit intercrystalline and dissolution-enlarged intercrystalline pores. Nevertheless, the parameter μ_{max} allows one to extract the "vuggy signal" from the T_2 spectra and subsequently identify those samples with vuggy pores.

The second parameter, σ_{main}, represents the standard deviation σ_i of the component with largest α. This parameter reflects the variance of the main pore size and can discriminate in particular intercrystalline (Figure 16A) and matrix micropores from the other pore types (Figure 16B) on the basis of their homogeneous pore sizes and attendant low σ_{main}.

Thus, 11 parameters were extracted from the NMR decomposition and used to discriminate different pore categories: α_i, μ_i, and σ_i from Eq. 3, μ_{max} and σ_{main}. The 11 parameters are presented for each sample in Appendix C.

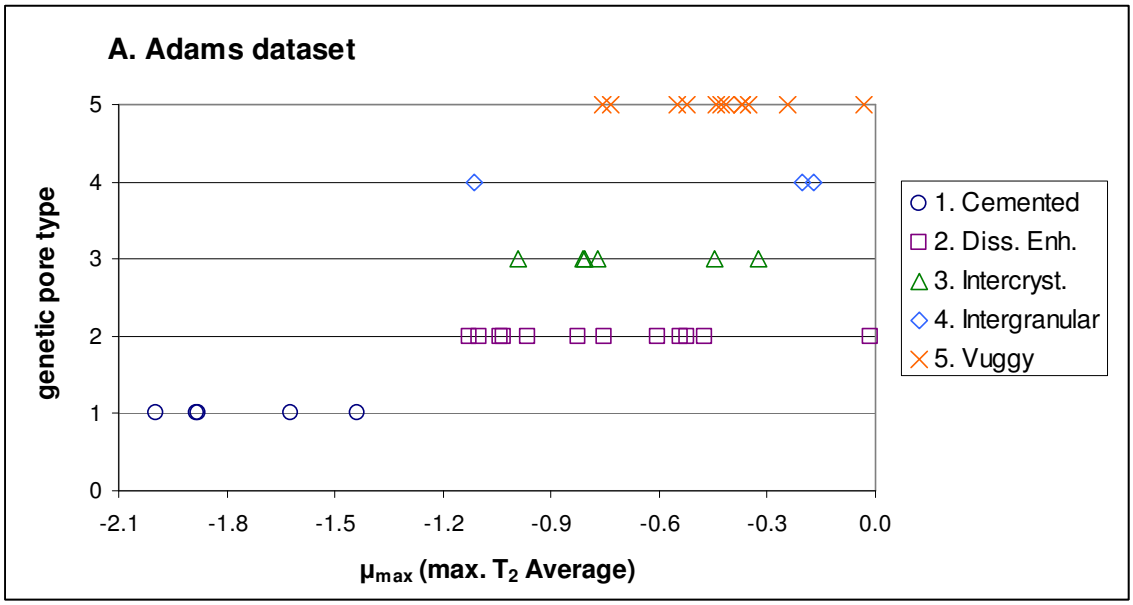

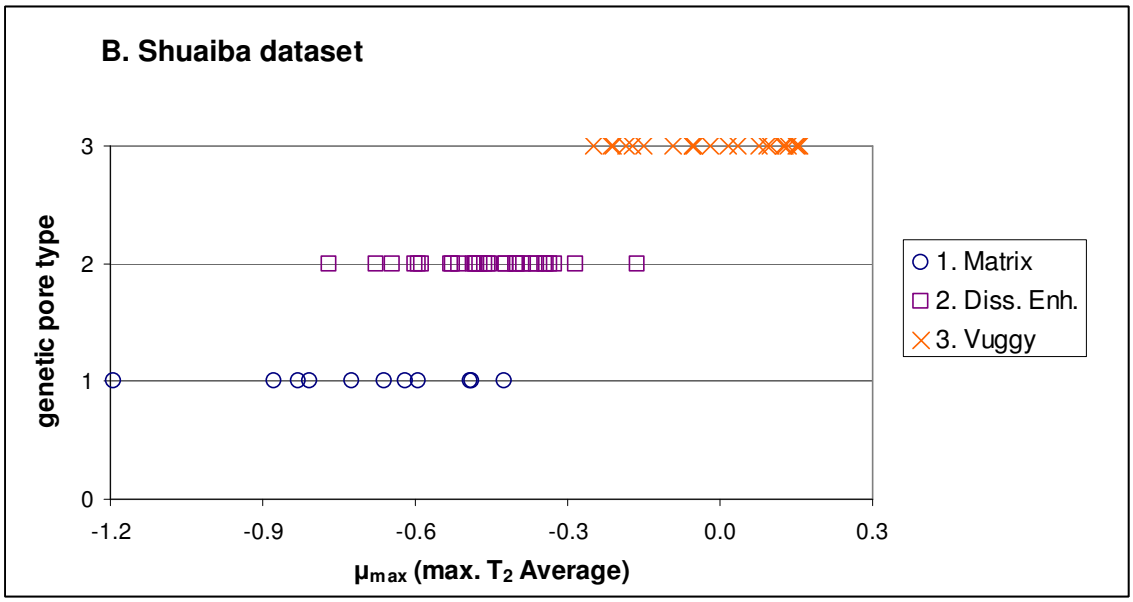

Figure 15: Univariate plots showing μ_{max} values for each pore type. A. Adams dataset, B. Shuaiba dataset

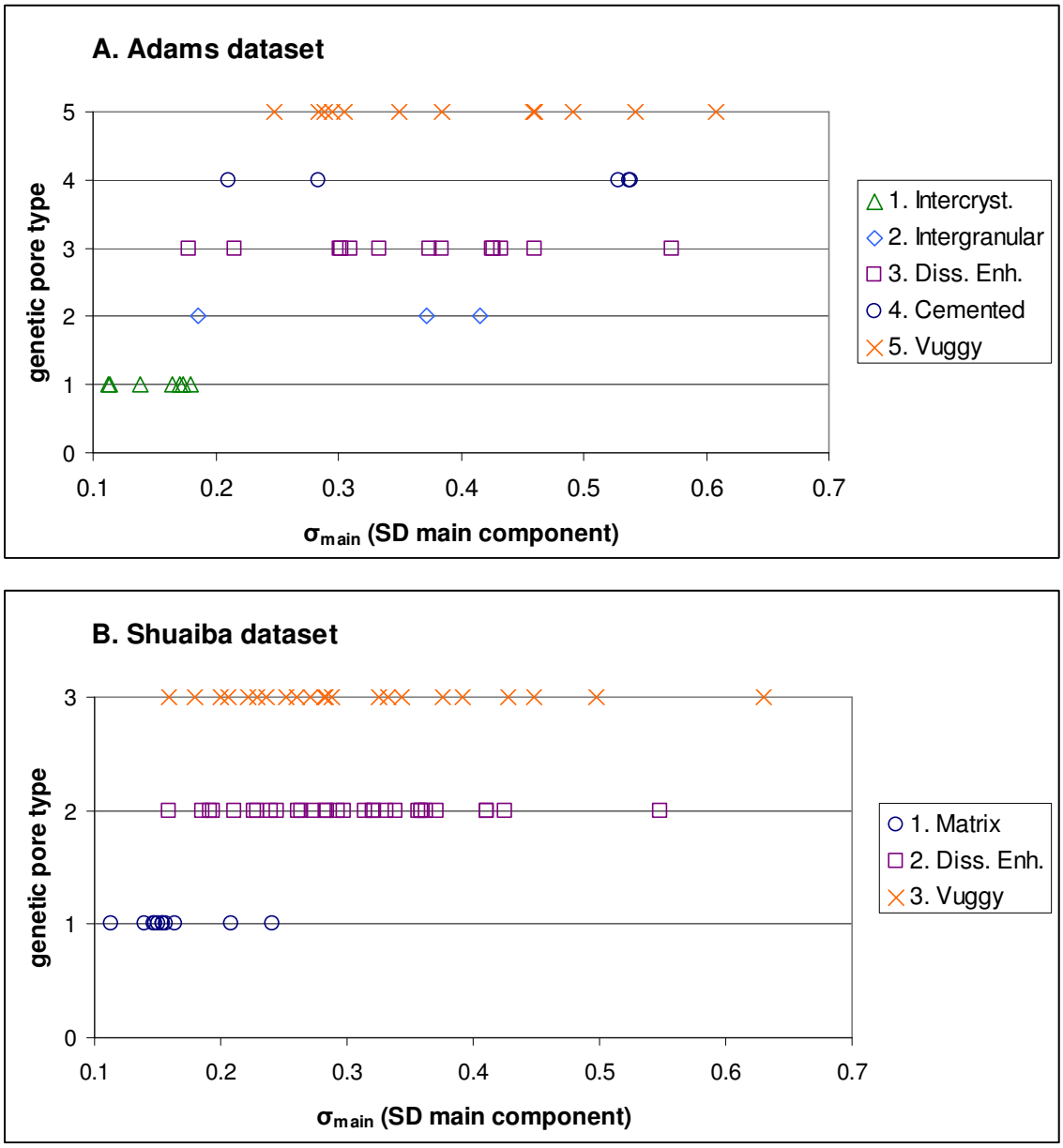

Figure 16: Univariate plots showing σ_{main} values for each pore type. A: Adams dataset, B: Shuaiba dataset

Not all 11 values were found to be useful in identifying the dominant pore types from the NMR response. For example, all three α's are not necessary, since they sum to one. The discriminatory power of these 11 variables was tested to choose the ones that are most useful in extracting the individual pore 'identities' from the NMR signature. Univariate plots of μ_{max} and σ_{main} (Figure 15- Figure 16) were compared to similar plots for the α_i, μ_i, and σ_i, with the result that μ_{max} and σ_{main} were found to have the greatest potential for distinguishing pore types from T_2 spectral decomposition. Plotting them together on a bivariate plot makes the pore categories appear in small, separate clusters (Figure 17). This outcome supports the decision to use μ_{max} and σ_{main} as key parameters to distinguish between pore types.

Finally, the discrimination routine STEPDISC was employed, as explained in Chapter IV, to test the assumption that μ_{max} and σ_{main} serve as the best parameters to discriminate pore types. The one variable that was found to be the most reliable discriminator of pore types was μ_{max} because it had the highest F value for both Adams and Lodola's datasets (Appendix D), confirming that μ_{max} is a key parameter for discriminating between genetic pore types.

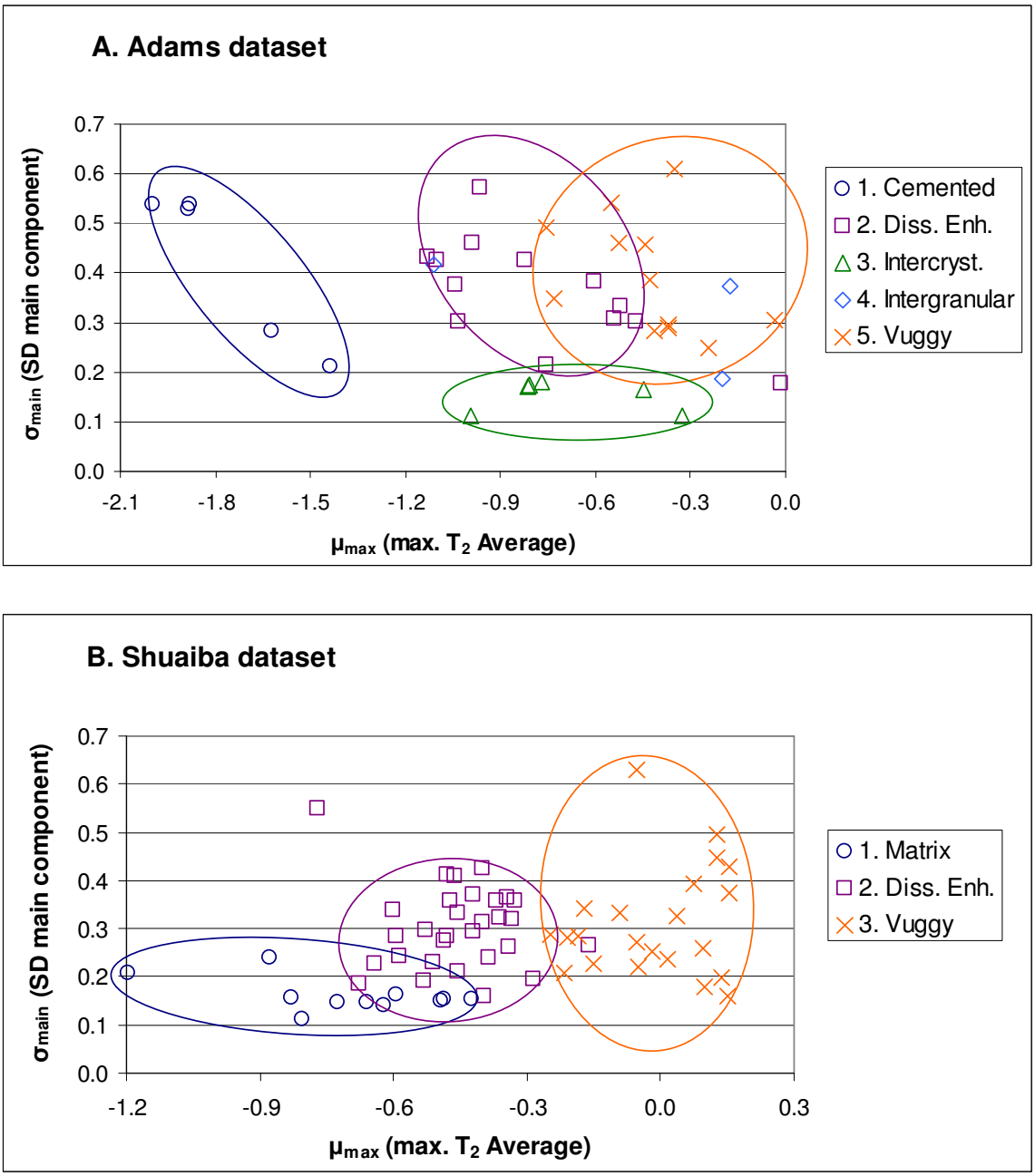

Figure 17: Bivariate plot of the two key parameters μ_{max} vs. σ_{main}. A: Adams dataset, B: Shuaiba dataset

The second key variable chosen is σ_{main}. The two final parameters that are retained in the statistical method, i.e. μ_{max} and σ_{main}, when used together were found to be powerful tools to discriminate between genetic pore types. Indeed, μ_{max} was found to differentiate between small (matrix, cemented), medium (dissolution-enhanced, intercrystalline) and large (vuggy) pores (Figure 15; 17). In addition to discriminating by pore size, σ_{main} provides a more complete pore identification based on the variance of the dominant pore size. Intercrystalline and matrix pores in particular can be single out based on σ_{main} (Figure 16; 17). The efficiency of μ_{max} and σ_{main} to identify independent characteristics of pore types based on an analysis of their correlation coefficients is discussed later in this thesis (Chapter VI).

Application of Bayes' theorem for predicting pore types

Once the two key parameters μ_{max} and σ_{main} have been identified as the best discriminators between pore types, calculations can be made of the joint normal probability density function of the two variables based on Eq. 9 - Chapter IV. Then Bayes' theorem is applied (Eqs. 7 and 9), with the parameter X now equal to μ_{max} and Y to σ_{main}. Finally, the probability that any specific sample belongs to one of the six possible pore categories is calculated, based on the sample values for μ_{max} and σ_{main}. Eq. 6 is used in this calculation with the assumption that all *a priori* probabilities are equal in order to avoid bias. This was particularly necessary in processing the Adams dataset as it consists of samples from three different fields with different depositional and diagenetic characteristics and histories.

The resulting probabilities calculated for each sample of both datasets are given in Appendix E. The following Table 2 provides the success rates of the pore type predictions based on Bayesian probabilities.

Table 2: Success rates of the pore type predictions based on Bayesian probabilities. A: Adams dataset, B: Shuaiba dataset

A. Adams dataset	Cmted	Intergran	Intercrys	Diss.Enh	Vuggy	**Total**
# samples	5	3	7	13	12	**40**
# good predictions	5	1	7	8	10	**31**
% correct	100	33	100	62	83	**78**

B. Shuaiba dataset	Matrix	Diss.Enh	Vuggy	**Total**
# samples	11	30	22	**63**
# good predictions	11	26	21	**58**
% correct	100	87	95	**92**

The large values of correct predictions (Table 2) indicate that μ_{max} and σ_{main} are able to discriminate between most of the pore types. The Shuaiba dataset shows the highest rates of correct predictions, both when considering the whole dataset and the individual pore categories. These higher success rates are explained by the fact that the Shuaiba dataset has less variety than the Adams dataset, as all the samples come from one single well. On the other hand, the Adams dataset combines samples from three different fields and ten different wells. Moreover, the Adams dataset is split into more pore categories and each contains fewer samples than the Shuaiba dataset, which makes it more difficult to define the probability of each pore type accurately by its μ_{max} and σ_{main} distributions.

In order to further investigate the differences in the predicted outcomes between datasets and pore categories, an average probability was calculated by which a sample is assigned to its predicted pore type (Table 3) based on the values found in Appendix E.

Table 3: Average Bayesian probability by which each sample was assigned to a predicted pore type. A: Adams dataset, B: Shuaiba dataset

A. Adams dataset	Cmted	Intergran	Intercrys	Diss Enh	Vuggy	**Total**
# samples	5	3	7	13	12	**40**
Average proba	0.98	0.54	0.90	0.56	0.62	0.72

B. Shuaiba dataset	Matrix	Diss Enh	Vuggy	**Total**
# samples	11	30	22	**63**
Average proba	0.93	0.92	0.92	0.93

Values in Table 2 indicate that the procedure to predict pore categories is not equally successful for all categories. Many categories show very high rates of success (Table 2); that is, probability values close to one (Table 3), except for the intergranular, dissolution- enhanced and vuggy samples from the Adams dataset. Examination of predictions for those samples shows that all wrong predictions except one correspond to misclassifications into one of these three same pore categories (Appendix E). For example, whenever a vuggy sample got misclassified, it was always assigned to either the intergranular or dissolution-enhanced category. Figure 17A indeed shows that vuggy, intergranular and dissolution-enhanced pore types do not always exhibit clear boundaries because the three categories include larger pores compared to other pore types, and μ_{max} and σ_{main} calculated from NMR T_2 decomposition might not always be effective at separating them. Intergranular pores in the Adams dataset had large pores and μ_{max} values in the same range as those for dissolution-enhanced and vuggy pores. Additionally, a significant probability exists of mistaking vuggy pores for dissolution-enhanced pores and vice-versa because both pore types are formed by the same process. The differences between them are a matter of degree rather than kind and both pore types commonly exhibit similar geometrical characteristics and close μ_{max} values. Since the Shuaiba dataset contains more dissolution-enhanced and vuggy samples, they can be defined with more certainty and less overlap on a μ_{max} vs. σ_{main} plot (Figure 17B).

Therefore their predictions show highest rates of success (Table 2) or probabilities closer to one (Table 3).

Test of the performance of the predictions

The genetic pore type predictions described previously are based on the distributions of two key parameters μ_{max} and σ_{main} that were calculated from samples in the Adams and Shuaiba datasets. Predicted pore types were assigned to each sample in these datasets, a method known as the resubstitution method (Krzanowski, 2000). The success rates that were calculated (Table 2) are "apparent success rates". Samples used to calculate probabilities that individual samples belong to certain pore categories are then resubstituted into the classification rule to determine the predicted pore type. As a consequence, the same samples are used to both define the classification rule and evaluate its performance. Because the classification rule was developed from the datasets in order to offer maximum separation of genetic pore types, individual samples should have the least chance of being misclassified by this rule and this resubstitution method should overestimate success rates.

In order to obtain a more reliable estimation of the performance of this pore type prediction method, the method of "leave-one-out" (also called "cross-validation" method) was used (Krzanowski, 2000). Assuming that the dataset consisted of "n" samples, this method involves taking one sample at a time out of the dataset, calculating the distributions of the two key parameters μ_{max} and σ_{main} from the remaining (n-1) samples, and determining the predicted pore type for the excluded sample on the basis of probabilities computed from the (n-1)-samples dataset. The procedure is repeated, omitting each of the n samples one at a time. Finally a determination is made of the success rate expressed as the percentage of correct predictions of the excluded samples. This leave-one-out method provides more reliable estimates of success rates than the resubstitution method because each sample that is classified during each successive calculation was not used in the computation of the classification rule. Moreover, it can be expected that the μ_{max} and σ_{main} distributions are only slightly affected by taking one sample out of the dataset at a time.

The predicted pore type for each sample obtained from the application of the leave-one-out method is presented in Appendix E. The following Table 4 provides a summary of the success rates of the leave-one-out method on both Adams and Shuaiba datasets.

Table 4: Success rates obtained from the leave-one-out method. A: Adams dataset, B: Shuaiba dataset

A. Adams dataset	Cmted	Intergran	Intercrys	Diss Enh	Vuggy	**Total**
# samples	5	3	7	13	12	**40**
# good predictions	5	0	5	6	8	**24**
% correct	100	0	71	46	67	**60**

B. Shuaiba dataset	Matrix	Diss Enh	Vuggy	**Total**
# samples	11	30	22	**63**
# good predictions	10	26	21	**57**
% correct	91	87	95	**90**

Table 4 should be compared to Table 2 to see the success rates from the resubstitution and leave-one-out methods. As expected, the success rates are lower overall for the leave-one-out method than for the resubstitution method. However, such a conclusion does not apply equally among datasets and pore categories. First, the resubstitution method and leave-one-out method have similar success rates for the Shuaiba dataset regardless of the pore category considered. On the other hand, the success rate dropped from 78% to 60% when the entire Adams dataset was examined. This difference is explained by the fact that the Adams dataset includes samples from different geological settings, whereas the Shuaiba dataset is defined by a greater homogeneity of characteristics of each pore type because all samples come from a single well. The processes that created porosity existed to a similar degree for all samples in this dataset, hence a reduced variability of sample pore characteristics. This contributes to creating higher probabilities of misclassification in the Adams dataset, whereas the μ_{max} and σ_{main} distribution of each pore type is more robust in the Shuaiba dataset.

Results of the leave-one-out method were examined for each pore category in the Adams dataset. The lowest success rates occurred in samples with dissolution-enhanced, intergranular and vuggy pore categories (Table 4). This outcome is similar to that obtained by the resubstitution method (Table 2) for the same reasons: namely, dissolution- enhanced, intergranular and vuggy categories are difficult to discriminate because they commonly have similar sizes, which means they will have similar μ_{max} values. The number of samples available for each pore category also has an impact on the outcome. In general, there are fewer misclassifications between the dissolution-enhanced and vuggy categories in the Shuaiba dataset than in the Adams dataset, probably because there are 13 dissolution-enhanced samples in the Adams dataset and 30 in the Shuaiba dataset. Similarly there are 12 vuggy samples in the Adams dataset and 22 in the Shuaiba dataset. The greater the number of samples that represent a pore category, the greater the accuracy of the definition of μ_{max} and σ_{main} distributions for the pore types. Subsequently, the greater the accuracy of definition of those parameters, the more reliable the subsequent pore type predictions will be.

Intergranular pores from the Adams dataset had a zero rate of success by the leave-one-out method (Table 4). This is most likely due to an insufficient number of samples to define this pore category. There were indeed only three intergranular samples available. Taking out one sample out of this category only leaves two samples hence a low chance of defining an accurate μ_{max} and σ_{main} distribution for this pore type, which in turn leads to a low chance of correctly predicting the third left-out sample.

CHAPTER VI

DISCUSSION

This chapter presents discussions on the limitations of the two types of data that were used in the study, and the significance of the assumptions that were made when using NMR to predict genetic pore types. Finally, a synthesis is given of how the pore type prediction method used in this study can be applied to other reservoir studies.

THIN SECTION STUDY LIMITATIONS

The pore type classification used in the study is based on thin section analysis. For the Shuaiba dataset, only thin section photomicrographs were available; they have a limited resolution as compared to thin sections viewed through the microscope. Nevertheless, the high success rates obtained for the Shuaiba dataset (Table 2) indicate that the photographs were a reliable source of data to classify pore types.

Analysis of porosity based on thin sections only provides a restricted view of the studied formation; therefore, the accuracy of the pore classification might be reduced if the thin section is not representative of the most common rock type in heterogeneous reservoirs, if the 2D view provided by the thin section does not reflect true 3D shape of the pores, or if there is a significant amount of very small or very large pores that can not be adequately captured by thin section study.

Bowers et al. (1993) compared different types of sandstone intergranular pores classified by pore sizes either from image analysis or from NMR measurements. His results showed an overall good correlation between the two sources of data. However some discrepancies observed pointed to intra-sample heterogeneity as a potential cause for poor results because single views of thin section sectors did not provide accurate representations of total sample porosity and pore types as compared to NMR measurements. This potential problem with using thin section data may be a cause for some of the apparent misclassifications of pores in this study when using the pore type prediction method. Pore types predicted from NMR data might be more reliable for some samples than pore type described from thin sections because NMR measures the

full volume of the rock sample instead of a small slice. However, the NMR response might itself have some limitations if the dominant pore type changes within the rock sample, in which case the NMR measurement will represent an averaged response for the investigated volume. Utilizing a program of closely-spaced thin section sampling might help to ensure representative results.

ASSUMPTIONS ASSOCIATED WITH T_2 RELATIONSHIP TO PORE-SIZE

It was assumed in this study of NMR data that surface relaxation is the dominant process occurring during NMR acquisition (Chapter II). This is a very important assumption because it establishes that the T_2 relaxation time constant of each pore can be considered as proportional to its volume (see Eqs. 1 and 2). This in turn explains why the T_2 distribution curve can be interpreted as a pore size distribution curve.

Bulk fluid relaxation as it corresponds to brine relaxation (all samples were 100% brine saturated) was not taken into consideration; it was assumed to be constant for all samples. Diffusion relaxation was considered to be negligible - usually a reliable assumption except for gas reservoirs.

A second hypothesis on which Eq. 1 (Chapter II) is based is that each pore is in the fast-diffusion limit. This assumption means that self-diffusion of the liquid, which constantly brings non-relaxed protons to the pore wall and moves relaxed protons to the center of the pore, occurs much faster than surface-induced relaxation. Therefore, the liquid response to the magnetic field - and the subsequent relaxation - will be uniform across the pore as the field decays with time (Kenyon, 1997). This has been verified for cases where pores are small enough and surface relaxation mechanism slow enough that a proton crosses the pore many times before it relaxes (Coates et al., 1999). The pore-wall relaxation time is much longer in that case than the time a particle needs to diffuse across the pore.

The reliability of this assumption might become critical as pore size or surface relaxivity becomes large or as molecular self-diffusion decreases. Therefore, the characteristics of NMR T_2 signals could be influenced by certain types of fluids, grain surfaces or very large pore volumes. For example, the presence of paramagnetic

minerals such as pyrite or iron-bearing dolomite can cause a large increase in the surface relaxivity if they are present in significant proportions on the pore wall surfaces. In such cases, special equations may be required to interpret relaxation constants (Kenyon, 1997).

DISCUSSION OF PORE TYPE PREDICTION METHOD

A variety of statistical tests were applied to both datasets in the study in order to assess the impact of the assumptions that were made when developing pore type prediction method.

Test of independence of the two key parameters μ_{max} and σ_{main}

Tests of relevancy were made of picking μ_{max} and σ_{main} as the two key parameters on which the pore type prediction is based. μ_{max} was chosen as it was identified as the variable with the highest discriminatory power by the STEPDISC procedure (Chapter V; Appendix D). μ_{max} represents the largest average pore size of all pore categories identified by the T_2 decomposition. σ_{main} was associated to μ_{max} to add a parameter that represents the variability of the most abundant pore type. In order to test whether these two variables extract independent characteristics of the T_2 decomposition, a hypothesis test was made on the correlation coefficient $\rho(\mu_{max}, \sigma_{main})$ for each pore category of both datasets. This hypothesis test determines whether $\rho(\mu_{max}, \sigma_{main})$ is significantly different from zero with a confidence interval of 5% (Krzanowski, 2000). The detailed results of the test are presented in Appendix F. All pore categories show that the coefficient of correlation is not significantly different from zero except for the dissolution enhanced category of the Adams dataset, for which t-statistic it is slightly off the range of t-critical. Therefore we can conclude that the two key parameters μ_{max} and σ_{main} do not show significant correlation. This reinforces our choice of these two parameters to develop the pore type prediction method. As they seem to characterize two independent properties of the T_2 distribution, they will maximize the performance of the discrimination method.

Choice of 0.10 as cutoff for significant pore type component

As explained previously in Chapter V, α_{lim}= 0.10 was used as a "cutoff value" to define what a "significant pore type component" is. Then μ_{max} can be calculated for each sample as being the maximum component average μ_i that has a significant weight, based on this definition of cutoff value α_{lim}= 0.10. A weight α_i (Eq. 3) which has a value below 0.10 can be considered to be negligible. The 0.10 value was chosen based on interpretation of the T_2 spectra decomposition results, where it appeared that the μ_{max} value corresponding to the vuggy component of the spectra was typically associated with a weight above 0.10. The third component μ_3 for samples without vuggy pores showed an α_3 weight between 0 and 0.10. However in order to test how this cutoff value would influence the outcome of the pore type predictions, we re-applied the Bayesian probabilities method and varied α_{lim}= 0.10 by +/- 20%, i.e. by setting α_{lim} = 0.08 and setting α_{lim} = 0.12 (Table 5).

Table 5: Effect of varying α_{lim}= 0.10 by +/- 20% on the pore type prediction success rates. The shaded column corresponds to the base case used in this study (α_{lim}= 0.10)

A. Adams dataset	α_{lim}= 0.10	α_{lim}=0.08	α_{lim}=0.12
% correct with entire dataset	78	75	73
% correct with leave-one-out method	60	55	55

B. Shuaiba dataset	α_{lim}= 0.10	α_{lim}=0.08	α_{lim}=0.12
% correct with entire dataset	92	84	89
% correct with leave-one-out method	90	81	86

The result of varying α_{lim}= 0.10 by +/- 20% is that it decreases the success rates of predicting pore types for both datasets (Table 5). When the details of the α_{lim} effect were examined by pore category, it appeared that decreased success rates using the entire

dataset were the result of additional confusion (misclassifications) between vuggy and dissolution enhanced categories except in one sample. The reason for the decreased success rates is as follows: when α_{lim}= 0.08, the third component becomes significant for some dissolution-enhanced samples; consequently, the average μ_{max} value increases for the dissolution-enhanced category and causes some of the vuggy samples to be misclassified in the dissolution-enhanced category. When α_{lim}= 0.12, the third component becomes insignificant for some vuggy samples, making the average μ_{max} parameter decrease for the vuggy category and causing some dissolution-enhanced samples to be misclassified as vuggy samples. Finally, the results indicate that a value of 0.10 is probably close to the optimum value for definition of a "significant pore type component" and resulting calculation of μ_{max}.

For samples that show a significant third component from the T_2 decomposition corresponding to the vuggy pores, the cutoff value discussed above can be taken to represent the minimum proportion of vugs as a proportion of total porosity in order for the sample to be classified in the vuggy category. The 0.10 cutoff value corresponds to the observation made by Adams (2005) that all samples classified as vuggy had between 10% and 30% vuggy porosity as a fraction of total porosity. Adams' data were calculated from 2D area measurements using petrographic image analysis techniques; vugs were defined as any pore larger than 0.5 mm.

Comparison of the μ_{max} and σ_{main} distributions between Adams and Shuaiba datasets

The Adams and Shuaiba datasets were treated separately during this study. They are "structured" differently because the Adams dataset has forty samples from ten wells and the Shuaiba dataset has sixty-three samples from a single well. Merging them would probably have resulted in the influence of the Shuaiba dataset overwhelming the Adams set, thereby resulting in biased distributions of the μ_{max} and σ_{main} parameters. It is interesting to compare the results of the T_2 decomposition between the two datasets by focusing on the pore categories common to both sets, i.e. the dissolution-enhanced and vuggy pore types (Table 6).

Table 6: Comparison of μ_{max} values for Adams and Shuaiba datasets. A: dissolution enhanced pores, B: vuggy pores

A. Diss. Enh. pores	Adams dataset	Shuaiba dataset
Avg (μ_{max})	-0.77	-0.46
SD (μ_{max})	0.33	0.13
# samples	13	30

B. Vuggy pores	Adams dataset	Shuaiba dataset
Avg (μ_{max})	-0.43	-0.01
SD (μ_{max})	0.20	0.14
# samples	12	22

The μ_{max} average values from the 2 datasets are dissimilar. The average μ_{max} is characterized by higher values for the Shuaiba dataset, both for the dissolution enhanced (-0.77 in Adams vs. -0.46 in Shuaiba) and vuggy (-0.43 in Adams vs. -0.01 in Shuaiba) categories (Table 6; Figure 17). This is interpreted to be due either to differing pore characteristics between the two datasets within a given genetic pore category, or differences in NMR acquisition conditions. The NMR data for the Adams and Shuaiba samples come from two different labs that might have used different brine fluids to saturate the plugs. In order to test the hypothesis of differing values of μ_{max} due to differing pore characteristics, a comparison was made of the shift in μ_{max} average between the two pore categories. If the shift turned out to be similar between dissolution-enhanced and vuggy samples, then differences in μ_{max} values could not be interpreted as an effect of differing pore characteristics but rather as a consequence of varying conditions of lab NMR acquisition.

Details of the hypothesis test that was applied are listed in Appendix G. The following null hypothesis H_0 was tested: "the shift in μ_{max} values that occurs from Adams to Shuaiba datasets is identical for vuggy and dissolution-enhanced categories". A one-tailed t-test with a 5% significance level was applied. The t-statistic calculated is lower that the t-critical, therefore null hypothesis (H_0) was accepted. The value of the shift in μ_{max} is statistically similar between dissolution enhanced and vuggy samples, therefore differences in μ_{max} values between the two datasets seem to not depend on pore

type; thus the shift in μ_{max} values may be interpreted as a consequence of varying NMR acquisition conditions.

In order to further test this interpretation, the values of σ_{main} between the two datasets were compared (Table 7). If the differences between the Adams and Shuaiba sets consist only in a constant shift of the T_2 distribution as indicated in the previous test, then the σ_{main} values should be similar because they describe the variability of the main component and are independent from absolute T_2 values.

Table 7: Comparison of σ_{main} values for Adams and Shuaiba datasets. A: dissolution enhanced pores, B: vuggy pores

A. Diss. Enh. pores	Adams dataset	Shuaiba dataset
Avg (σ_{main})	0.36	0.30
SD (σ_{main})	0.11	0.09
# samples	13	30

B. Vuggy pores	Adams dataset	Shuaiba dataset
Avg (σ_{main})	0.39	0.31
SD (σ_{main})	0.12	0.11
# samples	12	22

The σ_{main} values are similar in both datasets for both dissolution- enhanced and vuggy samples (Table 7). A t-test was applied using the following null hypothesis H_0: "the σ_{main} average values from both datasets are equal". A two-tailed t-test at the 5% significance level was used, following Davis (2002). The results of this test are presented in the following Table 8.

Table 8: Results from the t-test comparing σ_{main} averages between Adams and Shuaiba datasets. A: dissolution enhanced pores, B: vuggy pores

	Diss. Enh.	Vuggy
t-statistic	1.83	1.97
t-critical (two-tailed, 5% significance level)	2.09	2.07
Conclusion	H_0 accepted	H_0 accepted

H_0 is accepted in both dissolution-enhanced and vuggy cases (Table 8). Therefore, average σ_{main} values are statistically equal in the two datasets. This reinforces the previous interpretation of results from comparisons of μ_{max} average values. The differences in T_2 values between the two datasets seems to follow a constant shift that may be the result of differing NMR acquisition conditions since the pore characteristics from NMR seem statistically identical between the two datasets for a given pore category. But because of this shift in T_2 values, the datasets were kept separate.

Interpretation of the NMR T_2 spectra decomposition

The pore type prediction method in this study is based on the assumption that the T_2 spectral decomposition produces components that each characterizes a specific pore type. However it is possible that two components could correspond to a single pore category if that category does not have a normal distribution. It was also assumed that the T_2 spectra could be interpreted as a pore size distribution. However, T_2 values actually correspond most closely to the ratio of pore surface to pore volume (Eq. 1). Therefore, the varying shape of different pore types could create different combinations of surface to volume ratio that might yield the same T_2 values and distribution.

The validity of the assumption that the T_2 spectral decomposition produces components that each characterizes a specific pore type, can be verified by assessing the outcomes of the pore type prediction method. High success rates based on two parameters σ_{main} and μ_{max} from the T_2 spectral decomposition were obtained (Table 2). R^2 values, comparing measured and fitted T_2 spectra, were also always in the range of 0.95 to 1 (Appendix C). These results indicate that decomposition of the T_2 spectra does

indeed successfully capture different T_2 components that correspond to the main genetic pore types of the samples. Calibration of the method by using samples from cored wells should always be used as in this study to obtain accurate interpretations of T_2 spectra decomposition and optimize the performance of the pore type identification method from the NMR signature.

The pore type prediction method was based on the classification of each sample into one unique genetic pore type. This might appear restrictive as samples from complex carbonate reservoirs typically show a variety of pore types. This is the case for most of the samples from the Adams and Shuaiba datasets. This can also be observed in NMR decomposition results where each of several normal components might reflect characteristics of different pore types. However, the pore type identification from NMR is meant to be applied to NMR measurements obtained from the logging tool; therefore, the resolution of the NMR signal will not be as high as the one obtained from the NMR data acquired in the lab. The T_2 spectra obtained from NMR logs may not reflect all pore types present in the interval with the precision that T_2 spectra obtained from lab measurements provide. Knowing this, it was necessary to retain only the dominant pore type that will probably have most influence on reservoir quality ranking and petrophysical behavior.

The assumption that the pore type prediction method developed in this study is efficient to characterize the main genetic pore types present in each sample was tested as follows. For each sample, the two weights associated with the two normal components from which σ_{main} and μ_{max} were derived were summed. That sum takes into account the two components from the decomposition of the T_2 spectra that are used to predict genetic pore types. Those components might be identical or distinct depending on whether σ_{main} and μ_{max} correspond to a single component, i.e. whether there is a secondary component besides the main one or not. That sum can be interpreted as the portion of total porosity involved in developing the pore type prediction method. The average of this sum is equal to 0.84 for the Adams dataset and 0.91 for the Shuaiba dataset. Because these two values are close to 1, it shows that the components used for

pore type prediction represent a large proportion of the total porosity and are therefore likely to have the dominant influence on reservoir quality ranking and petrophysical behavior. Using only one or two components from the T_2 decomposition is efficient to identify genetic pore type. The pore type that has the greatest influence on reservoir behavior will be identified and all significant components from the T_2 spectra interpretation will be included.

APPLICATIONS OF THE PORE TYPE PREDICTION METHOD

Pore type identification from NMR measurement

Pore-type predictions used in this study provide a new application of NMR measurements in carbonate reservoirs. The method consists of using NMR as a genetic pore type identification tool in wells where only wireline log information is available. The method should be applied as follows:

(1) Use a dataset made of samples from cored wells to calibrate the system
- Assign a genetic pore type to each sample based on thin section study
- Apply the decomposition routine on the NMR T_2 spectrum of each sample
- Calculate the two parameters σ_{main} and μ_{max} from the decomposition results and compute their joint probability density function for each identified pore category
- Test the discriminatory power of σ_{main} and μ_{max} by using the resubstitution and leave-one-out methods on the samples from cored wells

(2) Predict pore types for a dataset made of samples from uncored wells
- Apply the decomposition routine on the NMR T_2 spectra of each sample
- Calculate the two parameters σ_{main} and μ_{max} from the decomposition results
- Using the σ_{main} and μ_{max} distribution of each pore category computed in the first step, estimate the probability of each sample to belong to each of the identified pore category
- Assign the sample to the pore category that has highest probability

Conditions and limitations of the pore type identification method

Application of the pore-type prediction method as described in the previous section has limitations. First, the method is based on calibrating the NMR data against rock samples from cored wells in order to estimate the σ_{main} and μ_{max} joint distribution for each identified pore category. This information is needed to compute the probability of each sample to belong to a specific pore category. The more complex the reservoir, the more samples are needed to obtain an accurate distribution of σ_{main} and μ_{max}. This can be seen when comparing the success rates between Adams and Shuaiba datasets, where the larger number of samples combined with a reduced variety of possible pore types seemed to provide higher success rates in the Shuaiba case.

It might be possible to use σ_{main} and μ_{max} distributions calculated from reservoir X that had cored wells available, to predict pore types in a second reservoir Y that has no cores available. However, using σ_{main} and μ_{max} characteristic values from reservoir X for application in reservoir Y requires that the same pore types and mineralogy are present in both reservoirs. A second limitation is that the NMR data have to be acquired in the same manner under the same environmental conditions, and especially with the same type of fluid. If those conditions are met, then NMR data may be used to identify pore types in reservoirs with no core samples as long as the system was previously calibrated against cores in a field with similar rocks and similar pores. Analysis of the Adams dataset that represent samples from widely different geographical and stratigraphic locations suggests that each genetic pore type has a specific σ_{main} and μ_{max} characteristic values. This is why the discrimination by pore categories of samples from different locations still resulted in high success rates in the Adams dataset case.

The objective of this study is to apply a method based on NMR measurements of core plugs made under lab conditions, to NMR data acquired in the field from a logging tool. Such a ‘leap’ in precision of the methods imposes additional limitations on the outcomes. For example, when going from NMR data in the lab to NMR data from the field there are variations in fluid content and type in the formation such as the presence of hydrocarbons, high salinity brines, or others. The presence of hydrocarbons influences

the T_2 distribution. For example, large pores filled with high viscosity oils, along with small pores filled with brine may display similar low T_2 relaxation times and therefore be difficult to distinguish (Henderson, 2004). A variety of methods are available to discriminate between the signals from the different fluids that might coexist in a reservoir (Kenyon, 1997). They consist in adapting the NMR acquisition sequence by varying either the interecho spacing T_e, or the wait time T_w between pulsed sequences. They rely on contrast in physical properties between the fluids, such as polarization time or diffusion ability.

Another effect on NMR acquisition could come from log measurement affected by borehole environmental conditions. For example, in case of a fractured reservoir, if borehole breakout occurs where the fracture meets the wellbore, mud may fill the space and cause overestimated porosity from the NMR measurement with a biased T_2 spectra towards low T_2 (Logan et al., 1998). Therefore, interpretation of NMR measurements should be made carefully in this type of specific logging environments.

Identification of potential candidates for acid stimulation

Acid stimulation is commonly used to improve oil production from carbonate reservoirs. The primary objective of acidizing is to dissolve the formation rock within its pore spaces. A knowledge of available materials, chemical reactions at treating and well conditions, and reservoir properties is required so that an efficient acidizing treatment can be designed (Bradley, 1992).

An aqueous solution of hydrochloric acid (HCl) is most commonly used for carbonate acidizing treatments. Other acids, however, might be used or mixed with HCl in specific cases to prolong reaction times or dissolve materials normally insoluble in HCl. Although dolomite reacts more slowly than limestones, it also dissolves in HCl resulting in magnesium chloride soluble in the acid. At bottomhole pressures, there is only a small difference (a factor of 1.5 to 2) in the reaction rates of acid with limestone compared to dolomite.

Many factors influence the reaction rate of an acid, such as pressure, temperature, flow velocity, acid type and concentration, reaction products, area/volume ratio and rock

composition. An understanding of these factors is necessary as a guide for the design of the acid treatment. This study provides a method of pore type identification from NMR. Pore type can then be related to expected geometry of the flow path and area/volume ratio, therefore providing information on some of these parameters that affect the acid reaction with the formation.

The area/volume (A/V) ratio corresponds to the pore area in contact with a given volume of acid. The larger the pore size or the fracture width, the smaller the A/V ratio, the more time the acid needs to spend on the formation. The value of this ratio may vary widely depending on the pore type or fracture characteristics. Moreover, the spending time must also be related to the distance the acid penetrates before it is spent, which depends on the geometry of the flow path that influences flow velocity. Pore size distribution and pore geometry influence the type of flow channels created by acid reaction. In matrix acidizing, which corresponds to acid injected below hydraulic fracturing pressure in order to remove formation damage, a very high A/V ratio would make it very difficult to obtain significant penetration before the acid is spent. This could be the case for intervals with dominant matrix or cemented pores as described in this study.

Acid fracturing corresponds to injection of acid into the formation above hydraulic fracturing pressure, in order to increase the natural producibility of the reservoir. Flow occurs mostly through hydraulic fractures, however much of the fluid does penetrate the matrix along the fractures faces. Therefore, the initial physical texture of the rock still affects the efficiency of the acidizing treatment. Acid fracturing is required when the producing formation does not have enough original permeability. The pore types characterized by the largest pore sizes as described in this study, which are the intergranular, dissolution-enhanced and vuggy categories, might provide the most favorable pore size distribution and geometry for effective acid stimulation if the reservoir is identified as needing a permeability enhancing treatment. For example, acid fracturing might create new permeability paths or interconnect existing permeability streaks in the intervals where large pore sizes dominate. Pore types associated with less

favorable pore sizes and geometry (cemented or matrix categories) might still be targeted for acid fracturing treatment, but the characteristics of the formation might result in a limited improvement of the overall reservoir producibility.

Because of the heterogeneity of the size and shape of the pores which is characteristic of limestones, penetration of acid in the rock is not uniform and a "channeling" or "wormholing" effect occurs in the formation. The resultant effect is an enhanced acid penetration of the matrix. On the other hand, dolomitized reservoirs do not present this favorable effect since the pore structure is typically very homogeneous. The porosity is directly controlled by the size of the dolomite crystals and the resulting intercrystalline pore space.

CHAPTER VII

FUTURE WORK

Future work might further investigate several aspects of this study. First, the assumption of normality could be tested by plotting log-normal probability plots for the samples that had unimodal T_2 distributions (T_2 decomposition resulted in one component only). This would allow an additional way to test the accuracy of the T_2 modeling method, as it was already shown that the use multiple Gaussian distributions was an efficient way to model the T_2 distribution based on good to excellent fits to measured spectra (all calculated R^2 between 0.95 and 0.99). The second assumption of normality, which was made when using the joint normal probability density function to estimate μ_{max} and σ_{main} distribution, could be tested in a similar way.

Another aspect to investigate is the application of the pore type prediction method based on NMR data acquired in the field. As discussed previously, there might be some difficulties when going from NMR lab data to NMR field data. This is why a similar study based on NMR log data would be of interest.

The interpretation of pore type prediction results for each pore category has shown that intergranular pores were difficult to single out from other pore types (Table 2). Only three samples were available in that category. This did not permit defining characteristics of these pores as shown on thin section or T_2 distributions that would reflect that category. Intergranular pores had μ_{max} values that were similar to dissolution enhanced or vuggy pores, showing that they are characterized by high T_2 values or large pore sizes. Therefore, having a new dataset containing more samples with intergranular pores would help identify a specific characteristic of the pore size or T_2 distributions that could be used to discriminate them, if such a characteristic actually exists and if a feature from the NMR T_2 curve can be found to reflect this characteristic. However, it is generally difficult to find carbonate samples with purely depositional pores since carbonate reservoirs typically have undergone some modifications during diagenesis. Intergranular pores are not a common pore type in carbonates.

The analysis of the pore type prediction results has also shown that the number of samples available to compute the μ_{max} and σ_{max} joint distribution has an influence on the success of the pore type prediction. Therefore, it would be interesting to see how many samples are required to ensure a good definition of μ_{max} and σ_{max} for each pore category. The minimum number of samples that is required can be determined based on the coefficient of variation of the variables that are considered (μ_{max} and σ_{max}) which is specific to each pore category, as well as the tolerance level allowed on the difference between sample (estimated) and population (true) variable values (Jensen et al., 2000). This problem is of importance since the pore type identification method starts with a calibration on samples from cores before applying it to uncored wells. An indication of the required number of samples may help indicate how many cores and thin sections are needed for that initial calibration step.

Finally, another direction on which future work could focus is how information on pore type from one well location and depth might be extrapolated to adjacent areas and at field scale. The porosity classification used in this study permits correlation of NMR with genetic pore type. First the geological origin of each pore type needs to be identified. For example, vuggy pores are typically formed by dissolution that occurs at rock/water interfaces, i.e. at water table or at the surface, where large volumes of undersaturated water can dissolve large volumes of rock. Then one can review the stratigraphic history of the field area and tie genetic pore types to a succession of events. Genetic categories generally ‘cross-cut’ each other to provide a ‘relative time scale’ to reveal which came first 2nd, 3rd, etc. Thanks to the identification method of genetic pore type and therefore origin of porosity from the T_2 curve, which was the result of this study, extrapolation of pore facies at field scale can be made in a more reliable way using this understanding of successive geological events that created porosity. Finally, the extrapolation of information collected at one location to adjacent areas might be done based on a statistical comparison of data measured at different locations and different depths, which would be based on the semivariance between adjacent areas, and the interpreted history of the formation of reservoir porosity.

CHAPTER VIII

CONCLUSION

This study provides a new method for using NMR measurements to identify genetic pore types in carbonate reservoirs. Using two different datasets comprising a total of 103 samples taken from four different carbonate reservoirs, the study has demonstrated that two key parameters computed from the NMR signal have significant geological meaning and that statistical analyses reveal parameter characteristics that are specific to genetic pore type. The two parameters, μ_{max} (maximum T_2 average) and σ_{main} (standard deviation of main component), are incorporated into the following method for identifying genetic pore types.

NMR T_2 spectra were first modeled as the sum of three normal components, each ideally representing a genetic pore type. Among the parameters obtained from statistical decompositions of the NMR spectrum, μ_{max} and σ_{main} were identified as the parameters with the highest degree of geological significance that could be used to discriminate between pore types. μ_{max} and σ_{main} represent respectively the largest average pore size of all pore types identified in the sample, and the size variability of the most abundant pore type. The joint distribution of μ_{max} and σ_{main} for each pore category was then computed, from which calculations were made to determine the probability that a certain sample belonged to each of the pore categories. Each sample was assigned to the pore category with the highest statistical probability of belonging.

The accuracy of the method was investigated and high success rates were obtained, i.e. 78% and 92% of predictions were correct for the Adams and Shuaiba datasets respectively when using the resubstitution method (pore type prediction rule based on the entire dataset). This represents an important advance over existing studies as it allows for a quantitative interpretation of NMR data to predict carbonate pore types. Previous work established relationships between pore characteristics and shapes of T_2 spectra but no methods are known by which pore type predictions can be made using large datasets with a variety of different carbonate pore types.

This new method should be particularly useful to identify carbonate pore types in uncored wells using NMR log data only. Ideally, the method should include NMR measurements on cores for purposes of calibrating the system to establish a baseline with which to compare in wells that only have wireline logs available. This is particularly important when seeking to obtain reliable μ_{max} and σ_{main} joint distribution for each pore category present in the reservoir. Differences in NMR acquisition and differences in borehole environment must also be taken into account. The results of this study show that a larger number of samples from each pore category will ensure a more robust definition of μ_{max} and σ_{main} values and ultimately a more reliable discrimination for distinguishing genetic pore categories.

These promising results indicate that NMR measurements are useful identifiers of carbonate pore types. The value of the statistical methods developed in this study is that they offer ways to investigate the relationships between NMR measurements and genetic pore types in carbonate reservoirs. Success in this work takes us closer to identifying genetic pore types from NMR logs with minimal calibration against borehole cores and will enable us map complex reservoirs with accuracy never before achievable.

REFERENCES CITED

Adams, A. J., 2005, Relationships between observed pore and pore-throat geometries, measured porosity and permeability, and indirect measures of pore volume by nuclear magnetic resonance: Ph.D. dissertation, Texas A&M University, College Station, Texas, 277 p.

Ahr, W. M., D. Allen, A. Boyd, H. N. Bachman, T. Smithson, E. A. Clerke, K. B. M. Gzara, J. K. Hassall, C. R. K. Murty, H. Zubari, and R. Ramamoorthy, 2005, Confronting the carbonate conundrum: Schlumberger Oilfield Review, Spring, p. 18-29.

Alsharhan, A. S., H. al-Aasm, and M. G. Salah, 2000, Stratigraphy, stable isotopes, and hydrocarbon potential of the Aptian Shuaiba formation, U.A.E.: SEPM Special Publication, v. 69, p. 299-314.

Anselmetti, F. S., S. Luthi, and G. P. Eberli, 1998, Quantitative characterization of carbonate pore systems by digital image analysis: AAPG Bulletin, v.82, no. 10, p. 1815-1836.

Atchley, S. C., M. G. Kozar, and L. A. Yose, 1999, A predictive model for reservoir distribution in the Permian (Leonardian) Clear Fork and Glorieta Formations, Robertson Field Area, West Texas: AAPG Bulletin, v.83, no. 7, p. 1031-1056.

Ausbrooks, R., N. F. Hurley, A. May, and D. G. Neese, 1999, Pore-size distribution in vuggy carbonates from core images, NMR, and capillary pressure: Society of Petroleum Engineers Paper 56506, p. 1-14.

Benson, D. J., 1985, Diagenetic controls on reservoir development and quality, Smackover Formation of southwest Alabama: GCAGS Transactions, v. 35, p. 317-326.

Benson, D. J., E. A. Mancini, R. H. Groshong, J. H. Fang, L. M. Pultz, and E. S. Carlson, 1997, Petroleum geology of Appleton Field, Escambia County, Alabama: GCAGS Transactions, v. 47, p. 35-42.

Bowers, M.C., R. Ehrlich, J. J. Howard, W. E. Kenyon, 1993, Determination of porosity types from NMR data and their relationship to porosity types derived from thin section: Society of Petroleum Engineers Paper 26307, p. 1-46.

Bradley, H. B., 1992, Petroleum Engineering Handbook – Third Printing: Richardson, Texas, Society of Petroleum Engineers, 1422 p.

Bui, T. D., J. L. Jensen, and C. L. Hanks, 2006, Neural network modeling with sparse datasets: Petroleum Science and Technology, (in press).

Chang, C., H. Vinegar, C. Morriss, and C. Straley, 1997, Effective porosity, producible fluid, and permeability in carbonates from NMR logging: The Log Analyst, v. 38, no. 2, p. 60-72.

Coates, G. R., D. Marschall, D. Mardon, and J. Galford, 1997, A new characterization of bulk-volume irreducible using magnetic resonance: Presented at the 1997 SPWLA 38th Annual Logging Symposium, June 15-18, 14 p.

Coates, G. R., L. Xiao, and M. G. Prammer, 1999, NMR Logging Principles and Applications: Houston, Halliburton Energy Services, 233 p.

Davis, J. C., 2002, Statistics and Data Analysis in Geology – Third Edition: New York, John Wiley & Sons, 638 p.

Hammel, B.S., 1996, High resolution reservoir characterization of the Permian (Upper Leonardian) Spraberry Formation, Happy Spraberry Field, Garza County, Texas: M.S. thesis, Texas A&M University, College Station, Texas, 156 p.

Henderson, S., 2004, Nuclear Magnetic Resonance logging, *in* G. Asquith and D. Krygowski eds., Basic Well Log Analysis: AAPG Methods in Exploration 16, p. 103-113.

Hidajat, I., K. K. Mohanty, M. Flaum, and G. Hirasaki, 2004, Study of vuggy carbonates using NMR and X-ray CT scanning: Society of Petroleum Engineers Reservoir Evaluation & Engineering Paper 88995, p. 365-377.

Jensen, J. L., L. W. Lake, P. W. M. Corbett and D. J. Goggin, 2000, Statistics for Petroleum Engineers and Geoscientists – Second Edition: Amsterdam, Elsevier, 338 p.

Kenyon, W. E., 1997, Petrophysical principles of applications of NMR logging: The Log Analyst, v. 38, no. 2, p. 21-43.

Kenyon, W.E., H. Takezaki, C. Straley, P. N. Sen, M. Herron, A. Matteson, and M. J. Petricola, 1995, A laboratory study of nuclear magnetic resonance relaxation and its relation to depositional texture and petrophysical properties – Carbonate Thamama Group, Mubarraz Field, Abu Dhabi: Society of Petroleum Engineers Paper 29886, p. 477-502.

Krzanowski, W. J., 2000, Principles of Multivariate Analysis: A User's Perspective: Revised edition: New York, Oxford University Press, 586 p.

Lodola, D., 2004, Identification of pore type and origin in a Lower Cretaceous carbonate reservoir using NMR T_2 relaxation times: M.S. thesis, Texas A&M University, College Station, Texas, 67 p.

Logan, W. D., J. P. Horkowitz, R. Laronga, and D. W. Cromwell, 1998, Practical application of NMR logging in carbonate reservoirs: Society of Petroleum Engineers Reservoir Evaluation & Engineering, October, p. 438-448.

Mancini E. A., and D. J. Benson, 1980, Regional stratigraphy of upper Jurassic Smackover carbonates of southwest Alabama: GCAGS Transactions, v. 30, p. 151-165.

Mancini E. A., D. J. Benson, B. S. Hart, R. S. Balch, W. C. Parcell, and B. J. Panetta, 2000, Appleton field case study (eastern Gulf coastal plain): Field development

model for Upper Jurassic microbial reef reservoirs associated with paleotopographic basement structures: AAPG Bulletin, v. 84, p. 1699-1717.

Mancini, E. A., T. A. Blasingame, R. Archer, B. J. Panetta, J. C. Llinas, C. D. Haynes, and D. J. Benson, 2004, Improving recovery from mature oil fields producing from carbonate reservoirs: Upper Jurassic Smackover Formation, Womack Hill field (eastern Gulf Coast, U.S.A.): AAPG Bulletin, v.88, no. 12, p.1629-1651.

Mancini E. A., B. H. Tew, and R. M. Mink, 1990, Jurassic sequence stratigraphy in the Mississippi Interior Salt Basin of Alabama: GCAGS Transactions, v. 40, p. 521-529.

Mazullo, S. J., and A.M. Reid, 1989, Lower Permian Platform and Basin depositional systems, Northern Midland Basin, Texas: Controls on Carbonate Platform and Basin Development, SEPM Special Publication No. 44, p. 305-320.

Parra, J. O., C. L. Hackert, and L. L. Wilson, 2002, A methodology to integrate magnetic resonance and acoustic measurements for reservoir characterization: Report DE-AC26-99BC15203, Southwest Research Institute, Department of Energy, San Antonio, Texas, 147 p.

Roy, E. C., 1998, High resolution mapping of flow units for enhanced recovery program planning, Happy Spraberry Lime Field, Garza County, Texas: M.S. thesis, Texas A&M University, College Station, Texas, 91p.

Russell, S. D., M. Akbar, B. Vissapragada, and G. M. Walkden, 2002, Rock types and permeability prediction from dipmeter and image logs: Shuaiba reservoir (Aptian), Abu Dhabi): AAPG Bulletin, v. 86, no. 10, p. 1709-1732.

Shell International Exploration and Production B.V., and Schlumberger, 1999, Petrophysics Distance Learning Module – First Edition: The Hague, CD-Rom.

Yang, K. M., and S. L. Dorobek, 1995, The Permian Basin of West Texas and New Mexico: Tectonic history of a ‘composite’ foreland basin and its effect on

stratigraphic development, *in* S. L. Dorobek and G. M. Ross. eds., Stratigraphic Evolution of Foreland Basins, SEPM Special Publication no. 52, p. 147-172.

APPENDIX A

LOG-NORMAL PROBABILITY PLOTS OF PORE SIZE DISTRIBUTIONS OBTAINED FOR THE ADAMS DATASET

The following log-normal probability plots test the pore size distribution for an example of each pore type described in the Adams dataset. The pore size distributions were obtained by image analysis techniques (Adams, 2005). All four plots show a nearly straight-line behavior which demonstrates that these carbonate pore sizes are log-normally distributed.

The x-axis is not symmetrical as the first pore diameters that were measured were approximated to zero; therefore the log of pore diameter could not be calculated. Some plots show a small part of the curve that appears to be vertical, however the curve is actually steeply inclined and this is only a result of a large number of pores in the considered probability range.

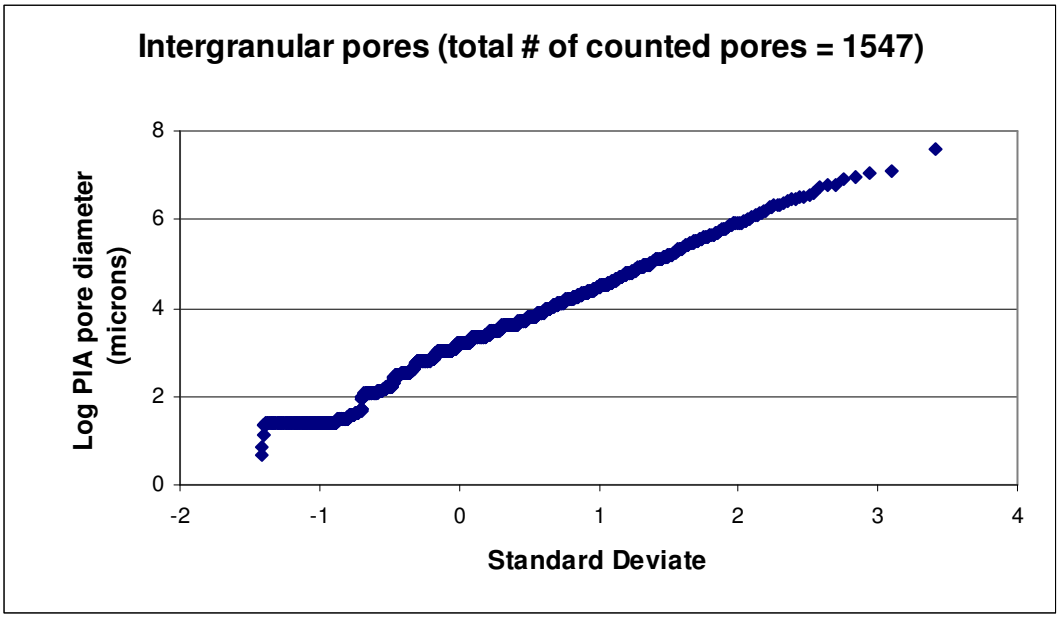

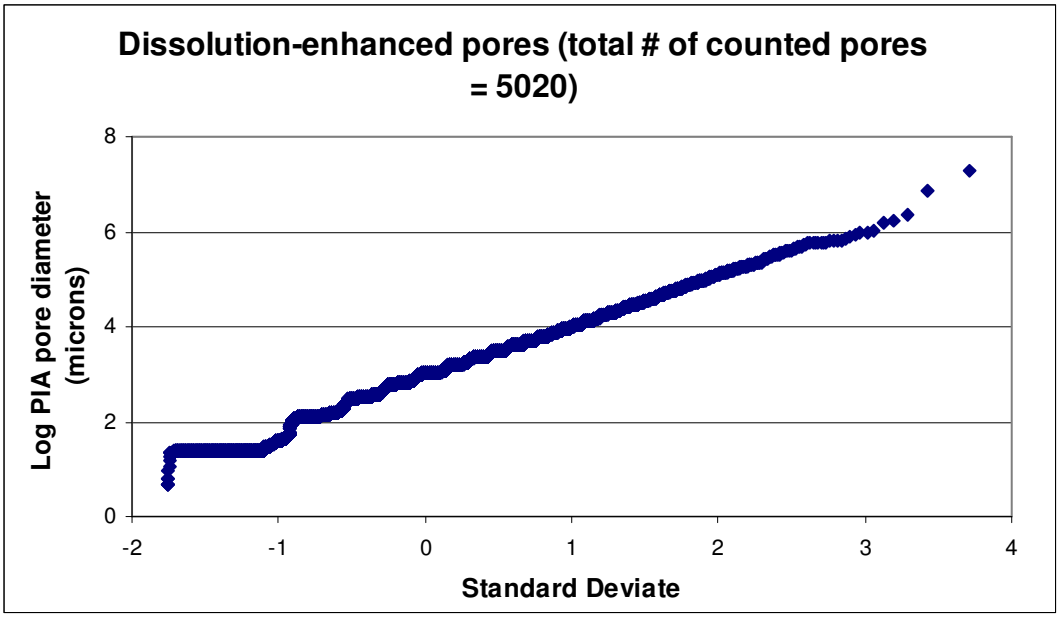
Dissolution-enhanced pores (total # of counted pores = 5020)
Log PIA pore diameter (microns)
8
6
4
2
0
-2
-1
0
1
2
3
4
Standard Deviate

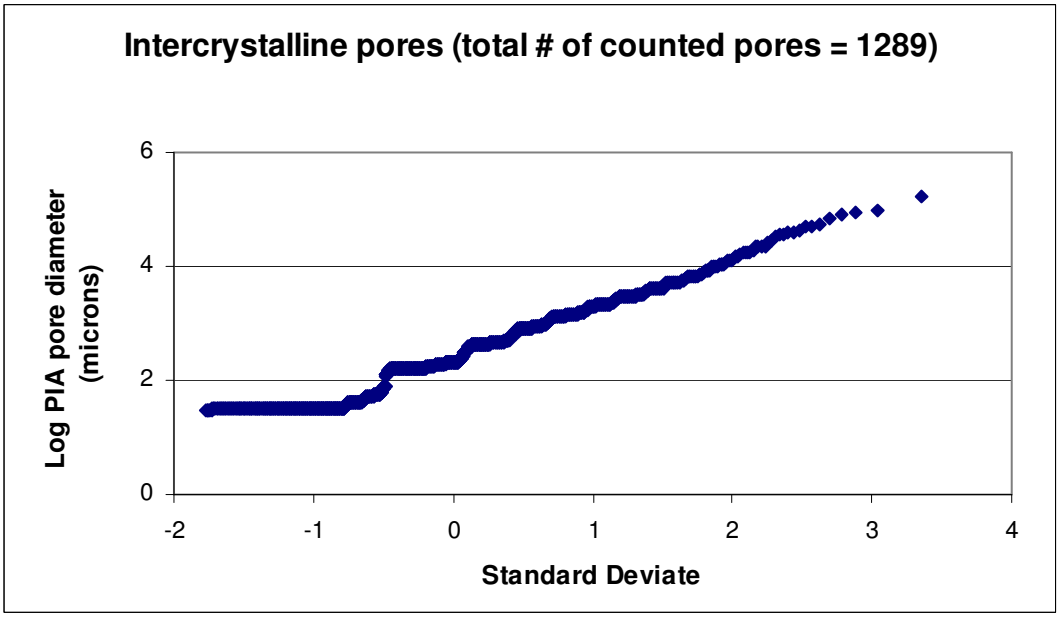
Intercrystalline pores (total # of counted pores = 1289)
Log PIA pore diameter (microns)
6
4
2
0
-2
-1
0
1
2
3
4
Standard Deviate

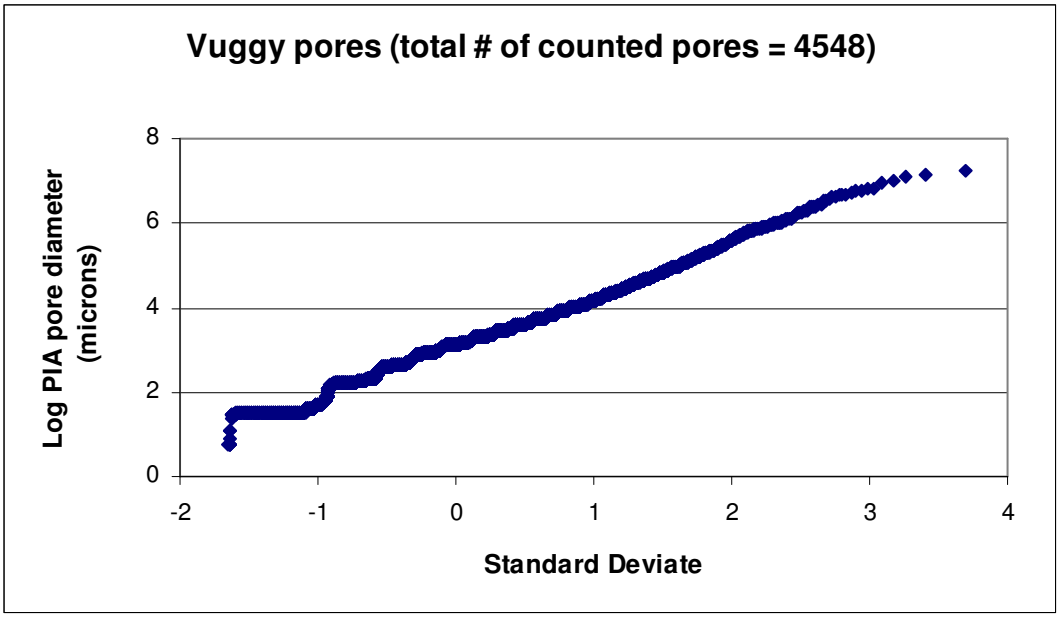
Vuggy pores (total # of counted pores = 4548)
Log PIA pore diameter (microns)
8
6
4
2
0
-2
-1
0
1
2
3
4
Standard Deviate

APPENDIX B

GENETIC PORE TYPE CLASSIFICATION BY SAMPLE ORIGIN

A. Adams dataset				
Producing Formation	**Field name**	**Well ID**	**Sample depth (ft)**	**Genetic pore type**
Permian Lower Clearfork, West Texas	Happy Spraberry Field	19-7	5,009.0	Cmted
			4,956.0	Diss. Enh.
		19-3	4,956.5	Diss. Enh.
			4,925.0	Diss. Enh.
			4,972.5	Diss. Enh.
			4,923.2	Diss. Enh.
Upper Jurassic Smackover, Alabama	Womack Hill Field	P4575	11,120	Vuggy
			11,129	Diss. Enh.
			11,146	Diss. Enh.
			11,156	Diss. Enh.
			11,174	Diss. Enh.
			11,192	Intercryst.
		P1591	11,405	Intercryst.
			11,411	Intercryst.
			11,413	Intercryst.
			11,515	Intercryst.
			11,528	Intercryst.
Upper Jurassic Smackover, Alabama	Appleton Field	3986	12,944	Cmted
			12,964	Vuggy
			12,970	Vuggy
			12,999	Vuggy
			13,024	Vuggy
		4633-B	12,868	Cmted
			12,948	Vuggy
			12,969	Diss. Enh.
			12,984	Vuggy
			13,014	Vuggy
			13,016	Vuggy
		3854	12,885	Cmted
			12,890	Cmted
			12,891.5	Vuggy

A. Adams dataset *(Cont.)*				
Producing Formation	**Field name**	**Well ID**	**Sample depth (ft)**	**Genetic pore type**
Upper Jurassic Smackover, Alabama	Vocation Field	2935	14,144	Diss. Enh.
			14,150	Diss. Enh.
			14,078	Intercryst.
		1599	13,987	Intergran.
			14,017	Intergran.
			14,059	Intergran.
			14,087	Diss. Enh.
			14,131	Vuggy
		5779	13,946	Vuggy

B. Shuaiba dataset				
Producing Formation	**Field name**	**Well ID**	**Sample depth (ft)**	**Genetic pore type**
Lower Cretaceous Shuaiba, Middle East	Unknown field	Unknown	8112.08	Diss. Enh.
			8114.70	Vuggy
			8116.42	Diss. Enh.
			8121.50	Vuggy
			8124.50	Diss. Enh.
			8125.17	Diss. Enh.
			8132.17	Vuggy
			8138.75	Diss. Enh.
			8141.83	Diss. Enh.
			8146.50	Vuggy
			8156.58	Diss. Enh.
			8171.00	Matrix
			8181.17	Diss. Enh.
			8184.46	Vuggy
			8200.08	Vuggy
			8208.17	Vuggy
			8213.25	Diss. Enh.
			8226.33	Vuggy
			8236.42	Vuggy
			8250.80	Diss. Enh.
			8254.92	Vuggy
			8256.00	Vuggy
			8256.50	Vuggy
			8257.00	Diss. Enh.
			8258.50	Diss. Enh.
			8282.00	Vuggy
			8312.00	Diss. Enh.
			8319.00	Diss. Enh.
			8358.58	Diss. Enh.
			8371.50	Diss. Enh.
			8385.50	Matrix

B. Shuaiba dataset *(Cont.)*				
Producing Formation	**Field name**	**Well ID**	**Sample depth (ft)**	**Genetic pore type**
Lower Cretaceous Shuaiba, Middle East	Unknown field	Unknown	8396.50	Matrix
			8447.70	Matrix
			8454.25	Matrix
			8461.80	Diss. Enh.
			8462.67	Diss. Enh.
			8476.00	Matrix
			8488.50	Vuggy
			8499.40	Matrix
			8522.50	Matrix
			8538.00	Diss. Enh.
			8551.20	Diss. Enh.
			8555.20	Diss. Enh.
			8604.25	Vuggy
			8604.92	Vuggy
			8608.67	Diss. Enh.
			8614.67	Diss. Enh.
			8620.50	Diss. Enh.
			8622.40	Vuggy
			8623.67	Vuggy
			8625.25	Vuggy
			8628.17	Diss. Enh.
			8635.10	Diss. Enh.
			8639.20	Vuggy
			8645.70	Vuggy
			8651.33	Diss. Enh.
			8657.50	Diss. Enh.
			8659.80	Diss. Enh.
			8663.70	Vuggy
			8664.50	Diss. Enh.
			8727.00	Matrix
			8745.50	Matrix
			8760.70	Matrix

APPENDIX C

PARAMETERS OBTAINED FROM NMR T_2 SPECTRA DECOMPOSITION

The following table summarizes the parameters that were obtained from the NMR T_2 decomposition according to Eq. 3 of Chapter IV: the three component means μ_i, standard deviations σ_i and relative weights α_i. In addition to these nine variables, the two variables μ_{max} and σ_{main} are highlighted in the table.

μ_{max} (highlighted in pink) corresponds to the maximum μ_i that has a significant weight, i.e. $\alpha_i > 0.10$. It enables to distinguish pore categories based on pore size, and will in particular help extract the vuggy pores signal from the T_2 spectra.

σ_{main} (highlighted in blue) is the standard deviation of the component with the largest weight, and therefore represents the variability of the most abundant pore size.

A. Adams dataset											
Pore type	**sample**	**Component 1**			**Component 2**			**Component 3**			**R^2**
		avg μ_1	**std dev σ_1**	**weight α_1**	**avg μ_2**	**std dev σ_2**	**weight α_2**	**avg μ_3**	**std dev σ_3**	**weight α_3**	
Cmtd	12868	-2.83	0.28	0.73	-1.62	0.16	0.17	-0.53	0.13	0.10	0.99
	5009	-2.90	0.09	0.00	-2.00	0.54	0.98	-0.68	0.09	0.02	0.99
	12885	-3.03	0.33	0.00	-2.22	0.54	0.72	-1.88	0.20	0.28	0.99
	12944	-2.69	0.24	0.36	-1.89	0.53	0.64	-1.38	0.42	0.00	0.99
	12890	-1.68	0.21	0.67	-1.44	0.12	0.33	-1.01	0.36	0.00	0.98
Inter-gran	14059	-2.23	0.36	0.33	-1.11	0.42	0.67	-0.01	0.44	0.00	0.99
	13987	-2.12	0.28	0.16	-0.83	0.42	0.28	-0.20	0.19	0.56	0.99
	14017	-2.22	0.56	0.27	-0.73	0.37	0.48	-0.17	0.13	0.25	0.98
Diss. Enh.	11156	-1.81	0.62	0.00	-0.54	0.31	1.00	-0.33	0.61	0.00	0.99
	11129	-1.53	0.15	0.01	-0.52	0.33	0.97	-0.19	0.08	0.02	0.99
	11174	-2.06	0.06	0.00	-0.60	0.38	0.99	-0.04	0.06	0.01	0.99
	11146	-1.05	0.10	0.00	-0.47	0.30	1.00	0.23	0.33	0.00	0.99
	4972.5	-1.95	0.30	0.29	-1.03	0.30	0.69	-0.80	0.09	0.02	0.99
	4956	-1.88	0.19	0.05	-1.13	0.43	0.95	-0.45	0.30	0.00	0.99
	4923.2	-0.70	0.25	0.23	-0.18	0.18	0.63	-0.01	0.08	0.14	0.99
	4925	-1.88	0.28	0.08	-0.82	0.43	0.91	-0.51	0.10	0.01	0.99
	4956.5	-2.21	0.30	0.00	-1.37	0.57	0.72	-0.96	0.19	0.28	0.99
	14150	-2.22	0.22	0.09	-1.10	0.43	0.91	-0.74	0.18	0.00	0.99
	14144	-2.28	0.31	0.00	-1.72	0.76	0.39	-0.75	0.22	0.61	0.99
	14087	-2.15	0.28	0.11	-1.04	0.38	0.89	-0.90	0.15	0.00	0.99
	12969	-2.28	0.37	0.09	-0.99	0.46	0.87	-0.63	0.14	0.04	0.99
Inter-crys	11192	-2.72	0.59	0.00	-0.99	0.64	0.20	-0.32	0.11	0.80	0.97
	14078	-2.01	0.60	0.36	-0.77	0.18	0.64	-1.08	1.28	0.00	0.98
	11405	-0.99	0.10	0.07	-0.64	0.16	0.83	-0.45	0.05	0.11	0.99
	11411	-1.45	0.22	0.11	-0.81	0.17	0.79	-0.65	0.05	0.10	0.99
	11413	-1.66	0.23	0.15	-0.81	0.17	0.85	-0.61	0.77	0.00	0.97
	11528	-1.53	0.38	0.09	-0.99	0.11	0.91	-0.36	0.55	0.00	0.95
	11515	-1.55	0.07	0.06	-0.71	0.14	0.94	-0.71	0.11	0.00	0.99

A. Adams dataset (*Cont.*)											
Pore type	**sample**	**Component 1**			**Component 2**			**Component 3**			**R^2**
		avg μ_1	**std dev σ_1**	**weight α_1**	**avg μ_2**	**std dev σ_2**	**weight α_2**	**avg μ_3**	**std dev σ_3**	**weight α_3**	
Vuggy	11120	-1.41	0.33	0.15	-0.37	0.29	0.85	-0.25	0.15	0.00	0.98
	14131	-2.16	0.48	0.20	-0.82	0.38	0.49	-0.43	0.15	0.31	0.98
	12970	-2.69	0.26	0.04	-1.29	0.48	0.29	-0.42	0.28	0.67	0.99
	12999	-2.27	0.19	0.03	-0.94	0.61	0.64	-0.35	0.21	0.33	0.99
	12964	-1.74	0.31	0.16	-0.73	0.35	0.84	-0.10	0.15	0.00	0.99
	13024	-2.65	0.21	0.05	-1.37	0.47	0.39	-0.37	0.30	0.55	0.97
	12891	-1.25	0.51	0.23	-0.46	0.30	0.49	-0.03	0.13	0.28	0.98
	13946	-1.83	0.43	0.20	-0.50	0.25	0.58	-0.24	0.12	0.21	0.99
	13014	-2.80	0.29	0.06	-1.12	0.54	0.68	-0.55	0.23	0.26	0.99
	13016	-2.23	0.26	0.10	-1.01	0.46	0.79	-0.44	0.13	0.11	0.99
	12984	-1.85	0.29	0.20	-0.76	0.49	0.76	-0.18	0.12	0.04	0.99
	12948	-2.41	0.21	0.07	-0.89	0.46	0.74	-0.52	0.17	0.20	0.99

B. Shuaiba dataset

Pore type	sample	Component 1			Component 2			Component 3			R^2
		avg μ_1	std dev σ_1	weight α_1	avg μ_2	std dev σ_2	weight α_2	avg μ_3	std dev σ_3	weight α_3	
Matrix	8171	-0.70	0.10	0.15	-0.42	0.15	0.85	-0.25	0.43	0.00	0.99
	8385.5	-0.75	0.08	0.11	-0.49	0.15	0.89	-0.17	0.47	0.00	0.99
	8396.5	-0.74	0.38	0.00	-0.49	0.15	1.00	-0.19	0.47	0.00	0.98
	8447.7	-0.60	0.13	0.05	-0.62	0.14	0.95	-0.09	0.50	0.00	0.98
	8454.3	-0.87	0.21	0.00	-0.88	0.24	1.00	0.11	0.05	0.00	0.99
	8476	-0.83	0.07	0.05	-0.59	0.16	0.95	-0.11	0.50	0.00	0.99
	8499.4	-2.16	0.01	0.00	-0.66	0.15	0.98	-0.50	0.03	0.02	0.99
	8522.5	-0.94	0.05	0.03	-0.72	0.15	0.97	-0.02	0.37	0.00	0.99
	8727	-1.46	0.43	0.00	-0.81	0.11	1.00	-0.77	0.13	0.00	0.98
	8745.5	-0.84	0.16	0.00	-0.83	0.16	1.00	0.00	0.40	0.00	0.99
	8760.7	-3.03	0.26	0.10	-1.19	0.21	0.90	0.61	0.49	0.01	0.98
Vuggy	8114.7	-1.02	0.21	0.06	-0.17	0.34	0.92	0.10	0.09	0.02	0.99
	8121.5	-1.38	0.39	0.12	-0.21	0.43	0.61	0.15	0.17	0.27	0.98
	8132.1	-0.86	0.10	0.01	-0.37	0.45	0.87	0.13	0.14	0.12	0.99
	8146.5	-1.00	0.21	0.12	-0.25	0.29	0.85	-0.02	0.08	0.03	0.99
	8184.4	-2.01	0.01	0.00	-0.46	0.28	0.72	-0.21	0.15	0.28	0.99
	8200.1	-0.86	0.22	0.14	-0.22	0.21	0.79	-0.03	0.07	0.08	0.99
	8208.1	-0.69	0.14	0.08	-0.56	0.42	0.19	0.15	0.16	0.73	0.99
	8226.3	-1.51	0.16	0.00	-0.33	0.39	0.88	0.08	0.13	0.12	0.99
	8236.4	-0.88	0.25	0.24	-0.15	0.23	0.70	0.05	0.08	0.06	0.99
	8254.9	-0.99	0.21	0.08	-0.27	0.33	0.81	0.04	0.12	0.10	0.99
	8256	-0.82	0.31	0.28	-0.05	0.22	0.65	0.15	0.08	0.07	0.99
	8256.5	-0.91	0.22	0.16	-0.19	0.28	0.78	0.06	0.10	0.07	0.99
	8282	-0.98	0.30	0.00	-0.53	0.53	0.36	0.10	0.18	0.64	0.99
	8488.5	-0.78	0.31	0.00	-0.61	0.38	0.56	0.15	0.18	0.43	0.99
	8604.2	-1.46	1.81	0.00	-0.83	0.63	0.56	-0.05	0.24	0.44	0.99
	8604.9	-1.26	0.31	0.20	-0.41	0.33	0.67	-0.09	0.13	0.14	0.99
	8622.4	-0.77	0.27	0.33	-0.02	0.25	0.60	0.19	0.09	0.06	0.99
	8623.6	-0.95	0.04	0.00	-0.71	0.26	0.85	0.09	0.14	0.15	0.99
	8625.2	-0.76	0.28	0.32	0.02	0.24	0.64	0.22	0.08	0.04	0.99
	8639.2	-1.02	0.20	0.09	-0.70	0.45	0.27	0.14	0.20	0.64	0.99
	8645.7	-0.81	0.25	0.29	-0.05	0.27	0.64	0.18	0.10	0.07	0.99
	8663.7	-0.93	0.14	0.03	-0.59	0.50	0.84	0.13	0.16	0.14	0.99

B. Shuaiba dataset (*Cont.*)											
Pore type	**sample**	**Component 1**			**Component 2**			**Component 3**			**R^2**
		avg μ_1	**std dev σ_1**	**weight α_1**	**avg μ_2**	**std dev σ_2**	**weight α_2**	**avg μ_3**	**std dev σ_3**	**weight α_3**	
Diss. Enh.	8112.1	-1.33	0.09	0.00	-0.48	0.41	1.00	0.46	0.52	0.00	1.00
	8116.4	-1.43	0.17	0.03	-0.37	0.36	0.97	-0.06	0.01	0.00	0.99
	8124.5	-1.68	0.01	0.00	-0.47	0.36	0.96	0.18	0.08	0.04	0.99
	8125.2	-2.81	0.07	0.00	-0.40	0.43	0.92	0.20	0.12	0.08	0.99
	8138.7	-1.05	0.15	0.03	-0.33	0.36	0.92	-0.02	0.11	0.05	0.99
	8141.8	-0.09	0.03	0.00	-0.34	0.36	1.00	-0.12	0.19	0.00	0.99
	8156.6	-0.78	0.28	0.00	-0.42	0.29	1.00	-0.25	0.31	0.00	0.99
	8181.2	-3.08	0.25	0.03	-0.67	0.34	0.34	-0.28	0.19	0.62	0.99
	8213.3	-1.47	0.01	0.00	-0.51	0.23	1.00	-0.54	0.24	0.00	1.00
	8250.8	-1.45	0.10	0.02	-0.36	0.32	0.94	0.31	0.11	0.04	0.99
	8257	-0.90	0.26	0.20	-0.16	0.26	0.72	0.08	0.10	0.08	0.99
	8258.5	-1.36	0.03	0.00	-0.39	0.24	1.00	-0.11	0.01	0.00	0.99
	8312	-0.69	0.37	0.00	-0.45	0.21	1.00	-0.29	0.33	0.00	0.99
	8319	-1.46	0.05	0.00	-0.34	0.26	0.97	-0.10	0.07	0.03	0.99
	8358.6	-0.64	0.29	0.00	-0.53	0.19	1.00	-0.19	0.48	0.00	0.99
	8371.5	-0.69	0.11	0.17	-0.40	0.16	0.83	-0.28	0.38	0.00	0.99
	8461.8	-0.72	0.01	0.00	-0.46	0.33	1.00	0.25	0.04	0.00	0.99
	8462.7	-1.42	0.11	0.03	-0.40	0.31	0.89	0.30	0.13	0.08	0.99
	8538	-0.46	0.01	0.00	-0.68	0.19	0.96	0.12	0.05	0.03	0.99
	8551.2	-0.90	0.04	0.00	-0.60	0.34	0.99	0.08	0.06	0.00	0.99
	8555.2	-1.40	0.09	0.00	-0.42	0.37	1.00	0.08	0.23	0.00	1.00
	8608.7	-1.88	0.01	0.00	-0.77	0.55	0.95	0.03	0.11	0.05	0.99
	8614.7	-9.72	7.84	0.00	-0.46	0.41	1.00	-0.16	0.04	0.04	0.99
	8620.5	-0.83	0.23	0.00	-0.59	0.28	1.00	0.11	0.03	0.00	1.00
	8628.2	-0.97	0.01	0.00	-0.64	0.23	1.00	0.16	0.03	0.00	0.99
	8635.1	-0.92	0.01	0.00	-0.33	0.32	1.00	-0.06	0.01	0.00	0.99
	8651.3	-0.81	0.25	0.00	-0.53	0.30	1.00	0.27	0.03	0.00	1.00
	8657.5	-3.05	0.04	0.00	-0.48	0.28	1.00	-0.26	0.01	0.00	1.00
	8659.8	-0.98	0.04	0.00	-0.59	0.24	1.00	-0.10	0.46	0.00	0.99
	8664.5	-0.76	0.04	0.00	-0.49	0.27	1.00	-0.40	0.18	0.00	1.00

APPENDIX D

STEPDISC DISCRIMINATION ROUTINE

Given a classification variable and several quantitative variables, the STEPDISC procedure performs a stepwise discriminant analysis to select a subset of the quantitative variables for use in discriminating among the classes. The set of variables that make up each class is assumed to be multivariate normal with a common covariance matrix.

The STEPDISC procedure that we applied was based on backward elimination. Variables are chosen to leave the model according to the significance level of an *F*-test from an analysis of covariance. Backward elimination begins with all variables in the model. Then at each step, the variable that contributes least to the discriminatory power of the model is removed. When all remaining variables meet the criterion to stay in the model, the backward elimination process stops.

The STEPDISC procedure was applied to the 11 variables available from the NMR T_2 decomposition: the three component relative weights α_i, means μ_i, and standard deviations σ_i, as well as μ_{max} and σ_{main} for each sample. The following results correspond to the final step of the backward elimination when no additional variable could be removed. They show that for both datasets, μ_{max} (see **) has the highest F value and consequently has the highest discriminatory power of all 11 initial variables (see Chapter 2 of Davis, 2002, for details on hypothesis tests).

A. Adams dataset	R^2	F value	Pr > F
σ_2	0.1907	1.83	0.1488
α_2	0.5759	10.52	<.0001
μ_3	0.2272	2.28	0.0832
μ_{max}	0.6225	12.78 **	<.0001
σ_{main}	0.5734	10.42	<.0001

B. Shuaiba dataset	R^2	F value	Pr > F
α_1	0.2677	10.24	0.0002
μ_2	0.3039	12.22	<.0001
σ_2	0.1956	6.81	0.0023
σ_3	0.1308	4.21	0.0197
μ_{max}	0.5718	37.39 **	<.0001

APPENDIX E

BAYESIAN PROBABILITIES AND RESULTING PREDICTED PORE TYPE

The following table presents the predicted pore type for each sample obtained by two different methods.

The first one relies on the entire dataset of n samples to compute the Bayesian probabilities from which a sample will be assigned to a pore category. It is called the resubstitution method. The probabilities that are presented in column 5 to 9 correspond to this resubstitution method. The resulting predicted pore type associated to the highest probability (which appears in red) is presented in column 10.

The second method relies on (n-1) samples to compute the probabilities after which the one sample that was left out is assigned to a pore category without having contributed to the definition of the pore type prediction rule. It is called the leave-one-out method. The resulting predicted pore type is presented in column 11.

Both methods are discussed in Chapter V of this study and Chapter 12 of Krzanowski (2000).

A. Adams dataset

Pore type	sample	μ_{max}	σ_{main}	Bayesian probabilities, n samples					Predicted pore type	
				cmtd	interg	diss enh	inter crys	vuggy	n samples	(n-1) samples
Cmtd	12868	-1.62	0.28	0.976	0.024	0.000	0.000	0.000	cmtd	cmtd
	5009	-2.00	0.54	0.989	0.010	0.001	0.000	0.000	cmtd	cmtd
	12885	-1.88	0.54	0.984	0.013	0.003	0.000	0.000	cmtd	cmtd
	12944	-1.89	0.53	0.985	0.013	0.002	0.000	0.000	cmtd	cmtd
	12890	-1.44	0.21	0.943	0.043	0.001	0.013	0.000	cmtd	cmtd
Inter-gran	14059	-1.11	0.42	0.000	0.284	0.713	0.000	0.002	diss enh	diss enh
	13987	-0.20	0.19	0.000	0.313	0.213	0.180	0.294	interg	vuggy
	14017	-0.17	0.37	0.000	0.348	0.068	0.000	0.584	vuggy	vuggy
Diss. Enh.	11156	-0.54	0.31	0.000	0.235	0.410	0.000	0.355	diss enh	diss enh
	11129	-0.52	0.33	0.000	0.220	0.353	0.000	0.428	vuggy	vuggy
	11174	-0.60	0.38	0.000	0.211	0.372	0.000	0.417	vuggy	vuggy
	11146	-0.47	0.30	0.000	0.232	0.344	0.000	0.423	vuggy	vuggy
	4972.5	-1.03	0.30	0.000	0.438	0.559	0.000	0.003	diss enh	interg
	4956	-1.13	0.43	0.000	0.274	0.724	0.000	0.002	diss enh	diss enh
	4923.2	-0.01	0.18	0.000	0.572	0.176	0.058	0.195	interg	interg
	4925	-0.82	0.43	0.000	0.242	0.633	0.000	0.125	diss enh	diss enh
	4956.5	-0.96	0.57	0.000	0.309	0.538	0.000	0.154	diss enh	interg
	14150	-1.10	0.43	0.000	0.271	0.726	0.000	0.003	diss enh	diss enh
	14144	-0.75	0.22	0.000	0.262	0.295	0.409	0.034	intercry	intercry
	14087	-1.04	0.38	0.000	0.303	0.692	0.000	0.005	diss enh	diss enh
	12969	-0.99	0.46	0.000	0.245	0.731	0.000	0.024	diss enh	diss enh
Inter-crys	11192	-0.32	0.11	0.000	0.112	0.072	0.735	0.081	intercry	interg
	14078	-0.77	0.18	0.000	0.047	0.033	0.917	0.003	intercry	intercry
	11405	-0.45	0.16	0.000	0.073	0.071	0.800	0.056	intercry	intercry
	11411	-0.81	0.17	0.000	0.031	0.017	0.950	0.001	intercry	intercry
	11413	-0.81	0.17	0.000	0.035	0.020	0.943	0.002	intercry	intercry
	11528	-0.99	0.11	0.004	0.032	0.002	0.962	0.000	intercry	interg
	11515	-0.71	0.14	0.000	0.019	0.009	0.970	0.002	intercry	intercry

A. Adams dataset (*Cont.*)										
Pore type	**sample**	**μ_{max}**	**σ_{main}**	**Bayesian probabilities, n samples**					**Predicted pore type**	
				cmtd	**interg**	**diss enh**	**inter crys**	**vuggy**	**n samples**	**(n-1) samples**
Vuggy	11120	-0.37	0.29	0.000	0.247	0.268	0.000	0.485	vuggy	vuggy
	14131	-0.43	0.38	0.000	0.192	0.165	0.000	0.643	vuggy	vuggy
	12970	-0.42	0.28	0.000	0.243	0.312	0.000	0.445	vuggy	vuggy
	12999	-0.35	0.61	0.000	0.098	0.001	0.000	0.901	vuggy	interg
	12964	-0.73	0.35	0.000	0.251	0.601	0.000	0.148	diss enh	diss enh
	13024	-0.37	0.30	0.000	0.244	0.259	0.000	0.498	vuggy	vuggy
	12891	-0.03	0.30	0.000	0.600	0.088	0.000	0.312	interg	interg
	13946	-0.24	0.25	0.000	0.319	0.238	0.001	0.443	vuggy	vuggy
	13014	-0.55	0.54	0.000	0.112	0.034	0.000	0.854	vuggy	vuggy
	13016	-0.44	0.46	0.000	0.152	0.069	0.000	0.779	vuggy	vuggy
	12984	-0.76	0.49	0.000	0.227	0.370	0.000	0.404	vuggy	diss enh
	12948	-0.52	0.46	0.000	0.157	0.115	0.000	0.729	vuggy	vuggy

B. Shuaiba dataset								
Pore type	sample	μ_{max}	σ_{main}	Bayesian probabilities, n samples			Predicted pore type	
				mtx	diss enh	vuggy	n samples	(n-1) samples
Matrix	8171	-0.42	0.15	0.742	0.252	0.006	mtx	mtx
	8385.5	-0.49	0.15	0.827	0.172	0.001	mtx	mtx
	8396.5	-0.49	0.15	0.844	0.155	0.001	mtx	mtx
	8447.7	-0.62	0.14	0.963	0.037	0.000	mtx	mtx
	8454.3	-0.88	0.24	0.981	0.019	0.000	mtx	diss enh
	8476	-0.59	0.16	0.918	0.082	0.000	mtx	mtx
	8499.4	-0.66	0.15	0.976	0.024	0.000	mtx	mtx
	8522.5	-0.72	0.15	0.991	0.009	0.000	mtx	mtx
	8727	-0.81	0.11	0.997	0.003	0.000	mtx	mtx
	8745.5	-0.83	0.16	0.999	0.001	0.000	mtx	mtx
	8760.7	-1.19	0.21	1.000	0.000	0.000	mtx	mtx
Vuggy	8114.7	-0.17	0.34	0.000	0.161	0.839	vuggy	vuggy
	8121.5	0.15	0.43	0.000	0.000	1.000	vuggy	vuggy
	8132.1	0.13	0.45	0.000	0.000	1.000	vuggy	vuggy
	8146.5	-0.25	0.29	0.000	0.618	0.382	diss enh	diss enh
	8184.4	-0.21	0.28	0.000	0.378	0.622	vuggy	vuggy
	8200.1	-0.22	0.21	0.016	0.362	0.622	vuggy	vuggy
	8208.1	0.15	0.16	0.001	0.000	0.999	vuggy	vuggy
	8226.3	0.08	0.39	0.000	0.000	1.000	vuggy	vuggy
	8236.4	-0.15	0.23	0.000	0.114	0.886	vuggy	vuggy
	8254.9	0.04	0.33	0.000	0.001	0.999	vuggy	vuggy
	8256	-0.05	0.22	0.000	0.010	0.990	vuggy	vuggy
	8256.5	-0.19	0.28	0.000	0.246	0.754	vuggy	vuggy
	8282	0.10	0.18	0.001	0.000	0.999	vuggy	vuggy
	8488.5	0.15	0.38	0.000	0.000	1.000	vuggy	vuggy
	8604.2	-0.05	0.63	0.000	0.000	1.000	vuggy	vuggy
	8604.9	-0.09	0.33	0.000	0.022	0.978	vuggy	vuggy
	8622.4	-0.02	0.25	0.000	0.004	0.996	vuggy	vuggy
	8623.6	0.09	0.26	0.000	0.000	1.000	vuggy	vuggy
	8625.2	0.02	0.24	0.000	0.002	0.998	vuggy	vuggy
	8639.2	0.14	0.20	0.000	0.000	1.000	vuggy	vuggy
	8645.7	-0.05	0.27	0.000	0.010	0.990	vuggy	vuggy
	8663.7	0.13	0.50	0.000	0.000	1.000	vuggy	vuggy

B. Shuaiba dataset (*Cont.*)								
Pore type	**sample**	**μ_{max}**	**σ_{main}**	**Bayesian probabilities, n samples**			**Predicted pore type**	
				mtx	**diss enh**	**vuggy**	**n samples**	**(n-1) samples**
Diss. Enh.	8112.1	-0.48	0.41	0.000	0.998	0.002	diss enh	diss enh
	8116.4	-0.37	0.36	0.000	0.972	0.028	diss enh	diss enh
	8124.5	-0.47	0.36	0.000	0.998	0.002	diss enh	diss enh
	8125.2	-0.40	0.43	0.000	0.985	0.015	diss enh	diss enh
	8138.7	-0.33	0.36	0.000	0.918	0.082	diss enh	diss enh
	8141.8	-0.34	0.36	0.000	0.948	0.052	diss enh	diss enh
	8156.6	-0.42	0.29	0.000	0.992	0.008	diss enh	diss enh
	8181.2	-0.28	0.19	0.105	0.656	0.239	diss enh	diss enh
	8213.3	-0.51	0.23	0.054	0.945	0.002	diss enh	diss enh
	8250.8	-0.36	0.32	0.000	0.967	0.033	diss enh	diss enh
	8257	-0.16	0.26	0.000	0.147	0.853	vuggy	vuggy
	8258.5	-0.39	0.24	0.004	0.972	0.024	diss enh	diss enh
	8312	-0.45	0.21	0.119	0.875	0.006	diss enh	diss enh
	8319	-0.34	0.26	0.000	0.938	0.061	diss enh	diss enh
	8358.6	-0.53	0.19	0.582	0.417	0.001	mtx	mtx
	8371.5	-0.40	0.16	0.674	0.313	0.013	mtx	mtx
	8461.8	-0.46	0.33	0.000	0.997	0.003	diss enh	diss enh
	8462.7	-0.40	0.31	0.000	0.987	0.013	diss enh	diss enh
	8538	-0.68	0.19	0.948	0.052	0.000	mtx	mtx
	8551.2	-0.60	0.34	0.000	1.000	0.000	diss enh	diss enh
	8555.2	-0.42	0.37	0.000	0.992	0.008	diss enh	diss enh
	8608.7	-0.77	0.55	0.000	1.000	0.000	diss enh	diss enh
	8614.7	-0.46	0.41	0.000	0.997	0.003	diss enh	diss enh
	8620.5	-0.59	0.28	0.000	0.999	0.000	diss enh	diss enh
	8628.2	-0.64	0.23	0.384	0.616	0.000	diss enh	diss enh
	8635.1	-0.33	0.32	0.000	0.935	0.065	diss enh	diss enh
	8651.3	-0.53	0.30	0.000	0.999	0.001	diss enh	diss enh
	8657.5	-0.48	0.28	0.000	0.998	0.002	diss enh	diss enh
	8659.8	-0.59	0.24	0.041	0.959	0.000	diss enh	diss enh
	8664.5	-0.49	0.27	0.000	0.998	0.002	diss enh	diss enh

APPENDIX F

HYPOTHESIS TEST ON CORRELATION COEFFICIENT

$\rho(\mu_{max}, \sigma_{main})$

The test on correlation coefficient $\rho(\mu_{max}, \sigma_{main})$ relies on the following property as explained in Chapter 14 of Krzanowski (2000):

If $\rho(X,Y)=0$ then $r\sqrt{[(k-1)/(1-r^2)]}$ has a t distribution on (k-1) degrees of freedom,

where $r(\mu_{max}, \sigma_{main})$ is the sample correlation coefficient, and k is the number of samples minus one.

Therefore we can apply a two-tailed t-test using the null hypothesis H_0: "$\rho(\mu_{max}, \sigma_{main})=0$". The following results show that in all cases except one, the t-statistic is within the t-critical range obtained from a table of values for the t-distribution at the 5% confidence level. Therefore, H_0 is accepted and $\rho(\mu_{max}, \sigma_{main})$ is found not to be significantly different from zero except for the dissolution enhanced category of the Adams dataset.

A. Adams dataset	Cmted	Intergran.	Intercryst.	Diss. Enh.	Vuggy
r (μ_{max}, σ_{main})	-0.78	-0.42	-0.12	-0.61	-0.37
k= n-1	4	2	6	12	11
t statistic	-2.14	-0.46	-0.28	-2.58	-1.26
t critical range (two-tailed test)	[-3.18, 3.18]	[-12.7, 12.7]	[-2.57, 2.57]	[-2.20, 2.20]	[-2.22, 2.22]
Conclusion	**accept Ho**	**accept Ho**	**accept Ho**	**reject Ho**	**accept Ho**

B. Shuaiba dataset	Matrix	Diss. Enh.	Vuggy
r (μ_{max}, σ_{main})	-0.46	-0.12	0.15
k= n-1	10	29	21
t statistic	-1.55	-0.61	0.70
t critical range (two-tailed test)	[-2.26, 2.26]	[-2.04, 2.04]	[-2.09, 2.09]
Conclusion	**accept Ho**	**accept Ho**	**accept Ho**

APPENDIX G

COMPARISON OF SHIFT IN μ_{max} VALUES BETWEEN THE TWO DATASETS

We observe that the average μ_{max} seems to be characterized by higher values for the Shuaiba dataset than for the Adams dataset, both for the dissolution enhanced and vuggy categories. This could be due to either varying pore characteristics or differences in NMR acquisition conditions. In order to test the hypothesis of differing values of μ_{max} possibly due to differing pore characteristics, we compare the shift in μ_{max} average between the two available pore categories. We test the following null hypothesis:

H_0: "the shift in μ_{max} values that occurs from Adams to Shuaiba datasets is identical for vuggy and dissolution-enhanced categories"

We use the values from the following table:

A. Diss. Enh. pores	**Adams dataset**	**Shuaiba dataset**
Avg (μ_{max})	-0.77	-0.46
SD (μ_{max})	0.33	0.13
# samples	13	30

B. Vuggy pores	**Adams dataset**	**Shuaiba dataset**
Avg (μ_{max})	-0.43	-0.01
SD (μ_{max})	0.20	0.14
# samples	12	22

We apply a one-tailed t-test with a 5% significance level. The t-statistic is calculated as follows:

$$t-stat = \frac{\mu_{\max} shift(Diss.Enh.) - \mu_{\max} shift(Vuggy)}{\sqrt{SE_{Diss.Enh.}{}^2 + SE_{Vuggy}{}^2}}$$

with

- μ_{max} *shift*= shift in μ_{max} average from Adams to Shuaiba datasets

hence

μ_{max} *shift* (*Diss.Enh.*)= (-0.77)-(-0.46)= 0.31

and

μ_{max} *shift* (*Vuggy*)= (-0.43)-(-0.01)= 0.42

- $SE = STANDARD\_ERROR = \frac{STANDARD\_DEVIATION}{\sqrt{\#\ samples}}$

hence

$$SE_{Diss.Enh.}{}^2 = \sqrt{SE_{Diss.Enh.,Adams}{}^2 + SE_{Diss.Enh.,Shuaiba}{}^2} = \sqrt{\left(\frac{0.33}{\sqrt{13}}\right)^2 + \left(\frac{0.13}{\sqrt{30}}\right)^2}$$

and

$$SE_{Vuggy}{}^2 = \sqrt{SE_{Vuggy,Adams}{}^2 + SE_{Vuggy,Shuaiba}{}^2} = \sqrt{\left(\frac{0.14}{\sqrt{22}}\right)^2 + \left(\frac{0.20}{\sqrt{12}}\right)^2}$$

We find that *t-stat* = 0.97, and t-critical= 1.64 obtained from a table of values of the t-distribution with a 5% confidence level and an infinite degree of freedom (the most restraining hypothesis). Therefore the t-statistic is lower that the t-critical and H_0 is accepted. The shift in μ_{max} average is statistically similar between dissolution-enhanced and vuggy samples.

VITA

Name: Coralie Genty

Permanent Address: Les Allogniers, 71960 La Roche Vineuse, France

Email Address : coralie_genty@hotmail.com

Education: M.Eng., Geology and Geological Engineering, Ecole Nationale Supérieure de Géologie, Nancy (France), 2004

M.S., Geoscience and Reservoir Engineering, Institut Français du Pétrole, Paris (France), 2006

M.S., Geology, Texas A&M University, College Station, Texas (U.S.A.), 2006

Professional Experience: Total Exploration and Production, Pau, France – Intern

EOG Resources, Denver, Colorado – Intern

ExxonMobil, Houston, Texas – Geologist